A Resource for the State of Florida

HURRICANE LOSS REDUCTION
FOR
HOUSING IN FLORIDA:

MITIGATION OF ROOF UPLIFT THROUGH VORTEX SUPPRESSION TECHNIQUES

A Research Project Funded by

The State of Florida Division of Emergency Management
Through Contract # 06RC-A%-13-00-05-261

Prepared by:

Arindam Gan Chowdhury, PhD & Collette Blessing, Research Graduate
Department of Civil and Environmental Engineering
Florida International University

In Partnership with:
The International Hurricane Research Center
Florida International University

August 2007

TABLE OF CONTENTS

CHAPTER **PAGE**

MITIGATION OF ROOF UPLIFT THROUGH VORTEX SUPPRESSION TECHNIQUES

Executive Summary

The objective of this study was to assess the effectiveness of modified roof edge geometry in the reduction of high suction pressures at roof corner and edge regions through full-scale testing approach. Utilizing the RenaissanceRe 6-fan Wall of Wind (WOW) testing apparatus at Florida International University (FIU), a test structure instrumented with pressure transducers was equipped with six different modified roof edge geometries and subjected to hurricane force winds. A series of seven tests, six for the different roof geometries and one to determine the standard pressure distribution without any modifications, were conducted and pressure data from all seven tests were compared. Results indicated that the use of such mitigation devices resulted in an average reduction in uplift by about 50%, with the largest reduction observed from the Flat Roof AeroEdge Guard (FRAG1, patent pending) which yielded 74% decrease in the worst suction in the corner region. Testing was also performed to identify the wind speeds at which the conical vortices became strong enough to start scouring different types of roof gravel. These results offer new hope for further development in the area of hurricane structural damage mitigation.

1. Introduction and Objective

Since the mid-1990s the North Atlantic Basin (defined as 0-30 degrees latitude) has experienced a substantial increase in tropical cyclone activity fueled primarily by warmer-than-usual sea surface temperatures and decreased wind shear. Proportional with increased frequency in hurricane land-fall is the increase in damage incurred and thus economic loss and loss of life. The annual average economic losses due to hurricanes increased from $1.3 billion in the years 1949-1989 to $10.1 billion from 1990-1995; with the occurrence of hurricanes Katrina and Rita, the 2005 season set a new record with losses totaling over $100 billion (Lott and Ross, 2006). The increase in annual losses is only projected to get worse; Risk Management Solutions (RMS) predicts a 40% increase in insured losses in Florida alone due to the above-normal tropical cyclone activity and associated damage (www.rms.com).

With approximately half of the United States population currently living within 50 miles of the coastline, the development of advanced structural mitigation techniques to protect communities against such devastating damage is an absolute necessity. The primary cause of roof failure during hurricanes is roof uplift due to severe negative pressures at roof edge and corner regions induced by vortex generation. Vortex generation refers to a process in which flow separation occurs as the wind flow meets a bluff body, such as a low-rise structure, and is forced to separate from the object. This separation stimulates the formation of a turbulent shear layer above the object where vortices build. These vortices then interact with the roof structure evoking strong negative pressure at edge and corner regions. As pointed out in the Institute for Business and Home Safety (IBHS) "Preliminary Damage Observation: Hurricanes Charley,

Frances, Ivan and Jeanne" (2004) 70-80% of all shingles and sheathing failure was initiated at the edge or corner regions by strong negative pressures associated with vortex generation.

Studies previously conducted using wind tunnels have shown that the application of modified roof edge shapes to a building can reduce, and in some cases even eliminate, the suction induced by vortex generation. The objective of this project is to conduct full-scale testing using the RenaissanceRe 6-fan Wall of Wind (WOW) to simulate hurricane force winds for the purpose of evaluating roof mitigation techniques. The WOW is not intended to replace other impact test methods but to complement current testing systems. This research proposes to evaluate in the full-scale the performance of three different prototype designs of modified edge shapes under hurricane-force winds and determine which design is most effective in reducing/eliminating negative pressure in the roof and corner regions. The ultimate goal of this project is to utilize the results of the above experiments to provide residents in hurricane-prone regions with alternative, cost-effective methods to better protect their homes.

2. Background: Vortex Suppression Initiatives

In an effort to reduce the catastrophic effects of hurricane force winds on residential and commercial roof structures several studies have set out to observe the effects of surroundings and alternative roof geometries on vortex generation. This innovative field of study is appropriately entitled "vortex suppression" as methods are currently being sought to disrupt and deflect the conical vortices from the roof structure to drastically reduce the effects of the extreme vortex-induced roof suctions. It is widely

believed that simple modifications in the shape of the roof edge may drastically reduce the vortex generation as well as associated damage (Surry and Lin, 1995).

For decades, parapets have been examined in wind tunnels as a means of vortex suppression simply because of their presence as a standard architectural feature. One of the first studies to specifically consider the role of these building components in vortex suppression was carried out by Baskaran and Stathopoulos (1988) at the Boundary Layer Wind Tunnel (BLWT) of the Building Aerodynamics Laboratory at Concordia University in Montreal, Canada. Researchers determined that parapets could have both positive and negative effects on suction pressure coefficients. The presence of parametric parapets at least 1 m in height proved effective in reducing pressure coefficients in the corner regions of buildings both 12 m and 96 m in height, however, the reduction was far more significant in the tall building variation ($\geq$ 96 m). This study also showed that the presence of parapets shorter than the 1 m critical height actually caused an increase in corner peak suctions. In general, the parametric parapet had a tendency to reduce corner pressure coefficients more significantly than a parapet present on only one side of the roof.

Parapet thickness was also found to reduce peak corner pressures in certain configurations. Researchers found that increasing the parapet thickness for the single-side parapet configuration demonstrated a decrease in the suction at the corner regions whereas only small reductions were observed in the parametric case.

Beyond examining parapets, recent studies have focused on developing modified roof edge shapes to be attached to the roof during preparations for high-wind events. Wu (2000) developed a modified roof edge shape called a Conical Vortex Disrupter in an

attempt to mitigate the extreme negative pressures caused by conical vortices. The device, installed at the roof corner at WERFL test building, effectively reduced suction pressures by 90% of the mean value and 80% of the peak value. Area averaged loads were also reduced by 50% for tributary areas smaller than 8.2 ft^2.

In the second portion of an experiment conducted by Lin and Surry (1993) which first examined the effectiveness of parapets in reducing suction, several roof corner geometry modifications were evaluated as means of mitigating vortex generation at the roof corner. The rounded roof edge displayed the most significant reductions in corner pressures reducing the peak, mean and rms pressure coefficients by more than 60%.

A follow-up study by Surry and Lin (1995), which also first examined the effects of parapets on roof suction, examined the effects of surroundings and several additional roof corner geometric modifications on roof pressures of low-rise buildings. Surry and Lin (1995) concluded that one of the primary factors affecting vortex intensity was surrounding terrain. In order to verify this theory, wind tunnel testing was conducted in which three different surrounding configurations were generated and tested with a 1:50 model of the TTU experimental building.

Results of this study indicated that the presence of surroundings changed the spatial distribution of pressure coefficients on the roof as well as significantly reduced the value in the corner regions for all three cases. Though the reduction of vortices due to the presence of surroundings was decidedly based on specific configurations of buildings, the presence of any configuration of surroundings generally lead to a reduction in magnitude of pressure coefficients of about 50-65%.

3. Methodology

3.1 The Wall of Wind Test Facility

Testing for this project took place at Florida International University using the RenaissanceRe 6-fan WOW full-scale testing facility. The RenaissanceRe 6-fan WOW is an expansion on the previous WOW (Figure 1), funded by the State of Florida Division of Emergency Management, which consisted of a 2-fan array of Chevy 496 fuel-injected engines driving airboat propeller shafts. The 2-fan WOW measures 16 ft tall and 8 ft wide, making it useful for individual component testing but limited in the fact that a test structure could not be fully engulfed in the flow due to size constraints.

Figure 1. 2-fan WOW System

The 6-fan WOW system came to fruition after the limitations of the prototype were realized (Figure 2). The larger WOW system consists of a 2x3 array of Chevy 502 big block carburetor engines turning Airboat Drive Units CH3 2:1 propeller drives. Measuring 16 ft tall by 24 ft wide, it is far more suitable for holistic full-scale testing than the prototype unit. The system is equipped with counter-rotating propellers, four large propellers closest to the engine and three smaller ones directly behind the others. The propellers limit the maximum revolutions per minute (rpm) of the engine to 4400. The four large propellers help to increase the air flow through the system while the three smaller propellers accelerate the flow. For this study, the back four propellers were set at a constant pitch of 15° while the three smaller propellers were set at 10°. This configuration of pitches allowed for the maximum amount of air flow through the system at the highest possible rpm. The counter-rotating function of the propellers helps to eliminate the swirl from the flow.

Figure 2. 6-fan RenaissanceRe WOW

Each engine is mounted in a steel frame measuring 96 in by 96 in. The frame is equipped with wedges in each corner to direct flow into the propellers. Each engine frame is then connected to an octagonal shaped diffuser which helps to minimize "dead zones" in the flow. "Dead zones" occur as a result of flow separation and often cause back flow which yields negative velocities in the wind field. The diffuser section is an integral part of ensuring an uninterrupted flow during testing.

The 6-fan WOW is currently capable of generating maximum wind speeds of 125 mph which represents a mid-grade Category 3 hurricane on the Saffir-Simpson hurricane intensity scale. The maximum rpm of each engine is approximately 4400 and 5500 with and without the propellers respectively. The scope of this project did not include turbulence effects in the wind field as the WOW is not currently equipped with a turbulence generator system. The turbulence generator system will be completed in 2007.

WOW Test Structure

All testing for this experiment was done using a plywood test structure measuring 10 ft x 10 ft x 10 ft. The test structure, equipped with standard window and door fixtures, rested on a square concrete pad and was secured to the ground using a system of guy wires. The test structure was placed at a 45° angle 9 ft from the edge of the WOW diffuser section and 16 ft from the back propellers for all testing (Figure 3). This distance allowed the flow to develop while keeping the structure close enough to the source of the flow so that it still experienced high velocity winds.

Figure 3. WOW Test Structure in Front of WOW at 45° angle

The structure was designed to withstand the maximum 125 mph winds generated by the WOW. For this experiment, the structure housed 16 pressure transducers, standard 1/4" nominal diameter peat rock gravel and a variety of different aerodynamic edge shapes. The top of the structure was coated with "Peel-N-Seal," a lightweight resilient, rubber-like product used primarily to patch holes in roofs following the passing of a hurricane. The "Peel-N-Seal" product acted as a weather-proofing device for the test structure to ensure that instrumentation did not get damaged from inclement weather or debris.

3.2 System Controls

WOW Controls

The six engines of the WOW were simultaneously controlled using LabVIEW algorithms developed by PrimeTest Automation. A manual ignition wired through the software provided a mechanism to turn the engines on after which the rpm of individual engines was directly controlled using the LabVIEW software. Each engine was equipped

with a Hightech HSR 5995 servo attached to the throttle, the physical mechanism that controls the rpm on the engine. A calibration curve correlated the position of the throttle to the servo position which was then in turn controlled by the researcher through the LabVIEW software. The position of the servo vs. rpm differed slightly from engine to engine so each engine had to be calibrated separately. This mechanism allowed the user the choice of running all engines at the same rpm or running select engines at different rpm. With the LabVIEW waveform editor, different rpm profiles were created and loaded into the program so that engines automatically adjusted rpm based on the function in the waveform. The waveform editor provided a more accurate mechanism for engines to quickly change speed, producing non-stationary gusts that are experienced in an actual tropical cyclone event.

The LabVIEW software helped to enhance the safety of the system by monitoring the performance of the six engines. A total of 48 thermocouples (eight for each engine) monitored the temperature of each cylinder in the engines. Senders attached to the engines and wired to the software monitored water temperature, oil temperature, oil pressure, voltage and rpm for each engine. Each of these elements had a range of values where operation of the engines was considered safe; the LabVIEW software monitored these values to make sure that threshold values were not reached.

In the case that any value would surpass the threshold values, an alarm on the channel caused the screen on the LabVIEW software reporting that particular parameter to turn red and engines were automatically restored to their idle rpm ranging between 750 and 1000 rpm depending on the engine. This function provided two advantages to the user: first, by programming the system to return the engines immediately and

simultaneously to idle rpm, engines were spared further damage that might have been incurred had a threshold value been reached and the operator was unaware; second, by turning the afflicting parameter red on the screen, the operator was made aware of which system parameter could potentially harm the engine and the problem could be properly addressed. The LabVIEW software program allowed the user the freedom to run different wind speed profiles while monitoring the safety of the engines to ensure efficient running of the system

Data Acquisition

The data acquisition (DAQ) system for the WOW was also developed by PrimeTest Automation using the LabView software (Figure 4). All pressure transducers and wind monitors were wired to the LabVIEW DAQ for data collection. The DAQ operated at a standard sampling rate of 200 Hz and data could either be collected continuously by manually triggering data record, or for a specified period of time.

Figure 4. WOW DAQ System

Calibration of instruments was also run through the DAQ. For pressure transducers, the DAQ was switched into a "calibration mode" where it was able to read raw voltages from the instruments. A hand-held Omega PCL-200C calibration kit generated known pressures and a calibration curve was established correlating the known pressures to the raw voltages read by the DAQ. This calibration curve was then added to the DAQ in spreadsheet format so that during testing, the DAQ would automatically convert voltages to pressures so that pressures were displayed on the screen and also stored.

The wind monitors were calibrated in a similar fashion as the pressure transducers. An anemometer drive unit generated a known rpm which was then related back to frequency changes read by the DAQ to create a calibration curve for the wind monitors. A further conversion of rpm to wind speed also took place so that the end result was a wind speed reading in miles per hour (mph). For calibration of the wind direction, a known excitation voltage was applied to the potentiometer and a calibration curve relating the known voltage to a wind direction was created. Calibration spreadsheets created in the DAQ were continuously read during data acquisition allowing the DAQ system to provide real-time plots of pressure and wind speed time histories during testing as well as continuously update the three-second average and instantaneous peak differential pressures and wind speeds.

3.3 Experimental Set-up

The following section provides a detailed description of the instrumentation used in this project as well as preliminary testing that was conducted in order to provide reference values for the primary experiments.

Instrumentation

Wind Monitors

This experiment required the use of four RM Young model 05103V wind monitors to measure the wind profile created by the WOW (Figure 5). Wind monitors were made of UV stabilized plastic with stainless steel and anodized aluminum fittings, making the instrument ideal for full-scale testing due to its durability. Each wind monitor recorded wind speed and direction with ranges between 0-224 mph and 0-360° respectively. The wind speed sensor consisted of a durable four-blade helicoid propeller which produced an AC sine wave voltage signal between 0-5 volts (V). As mentioned previously, the frequency of the sine wave was directly proportional to wind speed. The wind direction sensor was a lightweight vane with a low aspect ratio which made it an accurate reporting device for highly fluctuating winds. A potentiometer housed in a sealed chamber produces an output voltage directly proportional to the vane angle.

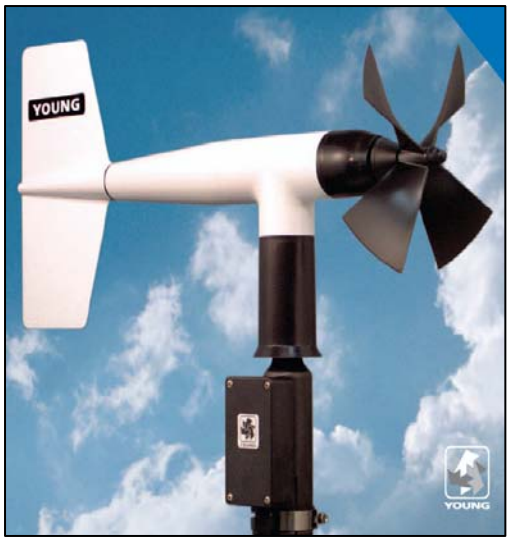

Figure 5. RM Young Wind Monitor

Pressure Transducers

Sixteen Setra model 265 very low differential pressure transducers were used for this project to measure the suction pressures on the roof induced by a hurricane-like wind flow (Figure 6). Each transducer had two ports, a reference pressure port and a port exposed to the roof of the test structure which measured the fluctuating pressures on the roof. The result was a differential pressure which reported into the DAQ as a voltage ranging from 0-5 V and was then calibrated and converted into psf (pounds per square foot). The transducers had a pressure range of ±1.8 psi or roughly ±260 psf (pounds per square foot) and reported at a frequency of 10 Hz and an accuracy of ±1 %.

Figure 6. Setra Model 265 Very Low Differential Pressure Transducer

The pressure transducers were connected to the reference pressure and dynamic pressure ports using a system of tubing. The reference pressure measurement was taken in a pressure pit located approximately 50 ft north-east of the corner of the test structure (Figure 7). A 3 in PVC pipe extended from the pressure pit into the test structure and was then reduced to a ¾" in PVC pressure manifold (Figure 8, Figure 9). The pressure manifold distributed the reference pressure to 16 different PVC ball valves. Each PVC ball valve was connected to 12 in piece of ¼ in ID (inside diameter) polyurethane tubing. The polyurethane tubing was connected to a piece of 240 in silicon tubing approximately 1/16 in ID via a plastic reduction fitting. This 1/16 in ID tubing was then attached to another piece of 1/4 in ID polyurethane tubing reduced to 3/16 in ID tubing which was attached to the actual reference pressure port (Figure 10). The additional reduction of the ¼ in ID tubing to the 3/16 in ID tubing was done because the port on the transducers had a 3/16 in diameter and accurate measurements required a secure fit of the tubing to the transducer. The 3/16 in ID tubing was not used initially because the small size of the tubing could have created more resonance if run the entire length of the connection. The

small silicon tubing connected between the larger polyurethane tubing served to filter out any noise cause by the resonance of the tubing and is therefore referred to as restrictor tubing.

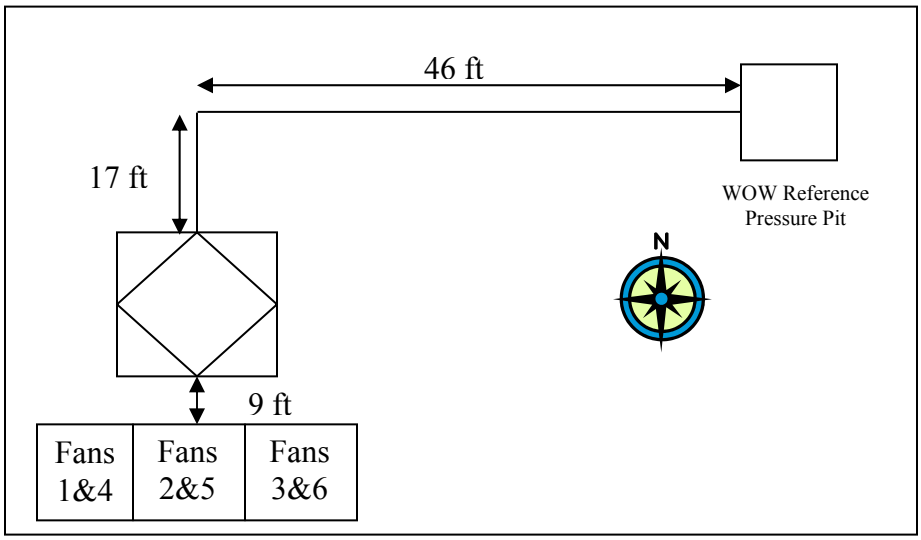

Figure 7. Schematic of WOW Pressure Pit Location

Figure 8. Three in PVC Pipe Extended from Reference Pressure Line

Figure 9. PVC Reference Pressure Manifold

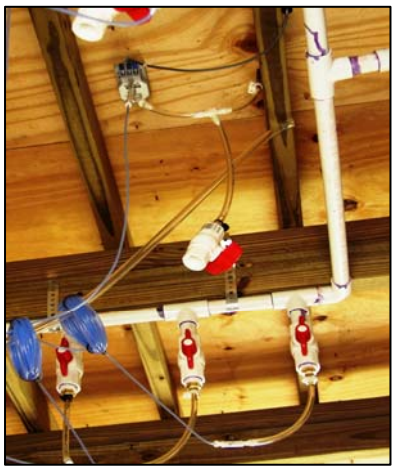

Figure 10. Pressure Transducer with Restrictor Tubing

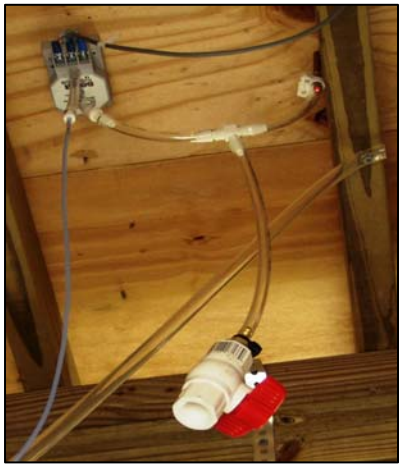

Figure 11. U-Shape Roof Port Connection for Prevention of Water Damage

The tubing system for the dynamic pressure port was much simpler. Here, the ¼ in ID polyurethane tubing was connected to a ¼ in OD (outside diameter) copper pressure tap which extended from the roof. The tubing then extended down where it was spliced into 2 different lines using a plastic ¼ in barbed "T" connection. One line of tubing ran straight down from the splice and was connected to another ball valve which served as a draining function should any water collect in the tubing. The other tube formed a U-shape and was then connected to the dynamic pressure port on the transducer (Figure 11). As with the reference pressure port, a small reduction of the ¼ in ID tubing to the 3/16 in ID tubing was placed directly before the pressure port to account for its smaller size. The total length of tubing that ran from the roof tap to the pressure port was restricted to a maximum of 12 in as longer tubing could have resulted in distorted measurements. The U-shape also served as a guard against water damage; in the event that water entered the system from the roof and flowed down to the ball valve and through the U-shape, it would never actually reach the pressure transducer because as it would have gotten trapped at the bottom of the U.

The extensive tubing system needed for the pressure transducers required two types of calibrations, a standard and dynamic calibration, to be performed to ensure a certain level of accuracy in the measurement. The standard calibration, mentioned previously in the *Data Acquisition* section, served two main purposes; first, it acted as a simple method to check that the pressure being fed into the pressure port was the same as that being reported through the DAQ, second, it helped to verify the factory calibration of the instrument which occurred at the time of assembly. Because initial calibrations indicated slight variation from the factory setting, a separate calibration was performed

on each transducer using the Omega PCL-200 hand held calibration kit before each experiment to ensure proper function of the instrumentation (Figure 12). The on-site calibration curve was used for each transducer to ensure the highest level of accuracy in the measurements. Figure 13 show the calibration curves for transducers 1-4 which are very similar to the factory calibration curve.

Figure 12. Omega PCL-200 Calibration Kit

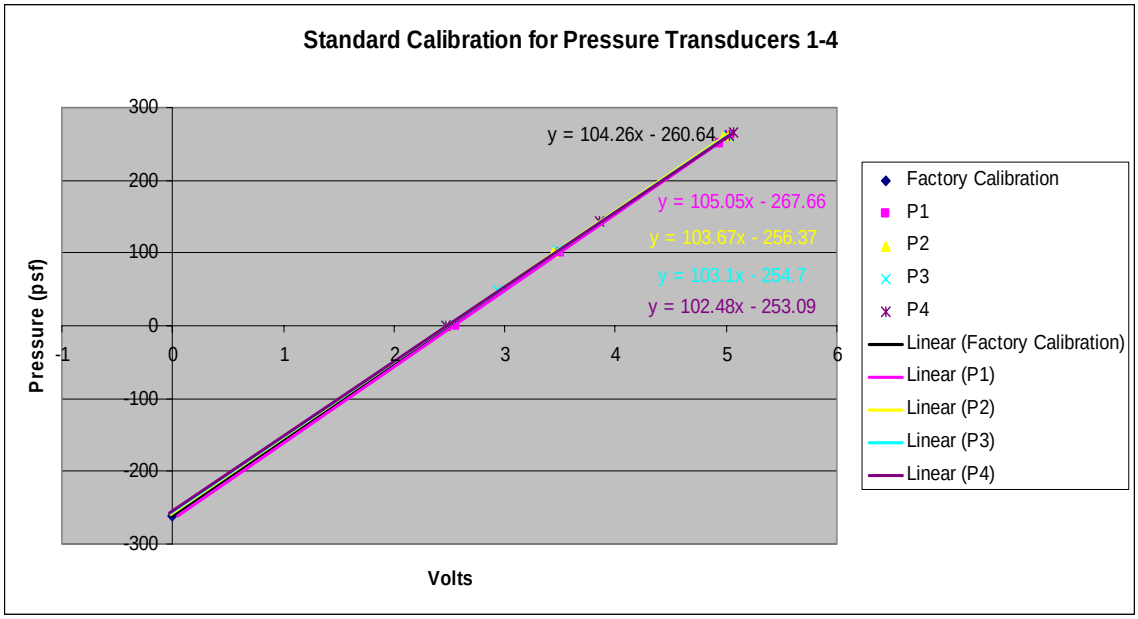

Figure 13. Example of Individual Calibration Curves for Pressure Transducers 1-4

The second type of calibration was a dynamic calibration. The dynamic calibration was performed on both the reference pressure port and roof pressure port (dynamic port). The purpose of the dynamic calibration was to evaluate the affects of the tubing lengths on the frequency response of the measurements. Previous testing has demonstrated that extended tubing lengths often result in amplitude and phase shifts thus distorting the measurement.

The dynamic calibration of the pressure transducers was achieved using a BK Precision Sweep Function Generator (SFG) and a standard audio amplifier and audio speaker. The SFG was attached to the audio amplifier which was then attached to the speaker. Two ¼ in holes were drilled into the speaker and a pressure transducer was attached to each of the two holes. The first pressure transducers was attached directly to one of the openings in the speaker via a small, ¼ in piece of tubing approximately 2 in long. The second transducer was attached to the remaining opening by a combination of

tubing beginning with a 2 in piece of ¼ in ID polyurethane tubing extending from the speaker. The ¼ in ID polyurethane tubing was then attached to 1/16 in ID silicone tubing using a plastic reducer fitting which was then increased a final time to a 2 in piece of 3/16 in ID polyurethane tubing that connected directly to the reference pressure port of the transducer (Figure 14). The SFG then generated a random function signal that was amplified by the audio amplifier and then applied to the pressure transducers via the speaker. The time histories resulting from the SFG signal were recorded by the DAQ.

Figure 14. Set-up for Dynamic Calibration of Pressure Transducers

Several different combinations of silicone and polyurethane tubing were tested, each time altering the length of the silicone tubing. The purpose of altering the length of the silicone tubing, or restrictor tubing, was to determine which length of tubing would appropriately remove all noise from the measurement. It was essential to remove noise form the reference pressure to assure that all differential pressure measurements referenced a uniform measurement. If this was not the case, measurements would have

varied greatly due to a fluctuating reference pressure measurement. First, the two transducers were tested directly attached to the speaker which resulted in two very similar fluctuating time histories. Next, 18 in, 24 in, 48 in, 72 in, and 120 in pieces of tubing were tested. With each increasing length, the amount of noise in the time history of the transducer attached to the speaker through tubing compared to the transducer attached directly to the speaker decreased. The last piece of tubing tested, a 240 in piece, was the most effective in dampening out noise and therefore was used for this experiment (Figure 15). By applying restrictor tubing to filter out high frequency noise, a transfer function did not have to be applied to the data to account for resonance in the tubing, thus no post-processing of data was necessary.

The dynamic calibration for the roof pressure port was much simpler and served only to verify that the 12 in tubing used did not cause significant phase and amplitude shift in the data. To achieve this calibration the same set-up of pressure transducers and speaker was used, however, one of the transducers was attached to the speaker with only a 12 in length of polyurethane tubing and no restrictor tubing. The SFG was used to generate sine waves over multiple frequencies and pressure time histories for the transducers were observed for each frequency. The two transducers measured very similar pressure time histories over all frequencies, and therefore no transfer function was needed for the roof pressure side of the transducers (Figure 16). The calibration performed for these experiments indicated that the tubing configurations specified above were appropriate for both the reference and roof pressure.

Reference Velocity Measurements

Before testing of the modified edge shapes was conducted, velocity measurements were taken to establish both the free-stream velocity profile produced by the WOW and a curve relating wind speed and engine rpm. In order to get the true free-stream velocity, all velocity profile measurements were taken without the presence of the test structure as the structure would have affected the wind field. These free-stream measurements provided information about the specific velocity values that would be present at the test structure eave height which was the focal point of the pressure testing and scour testing. By already knowing the velocity profile prior to testing, all pressure measurements could be directly related back to a wind speed without having to take simultaneous pressure and wind speed measurements.

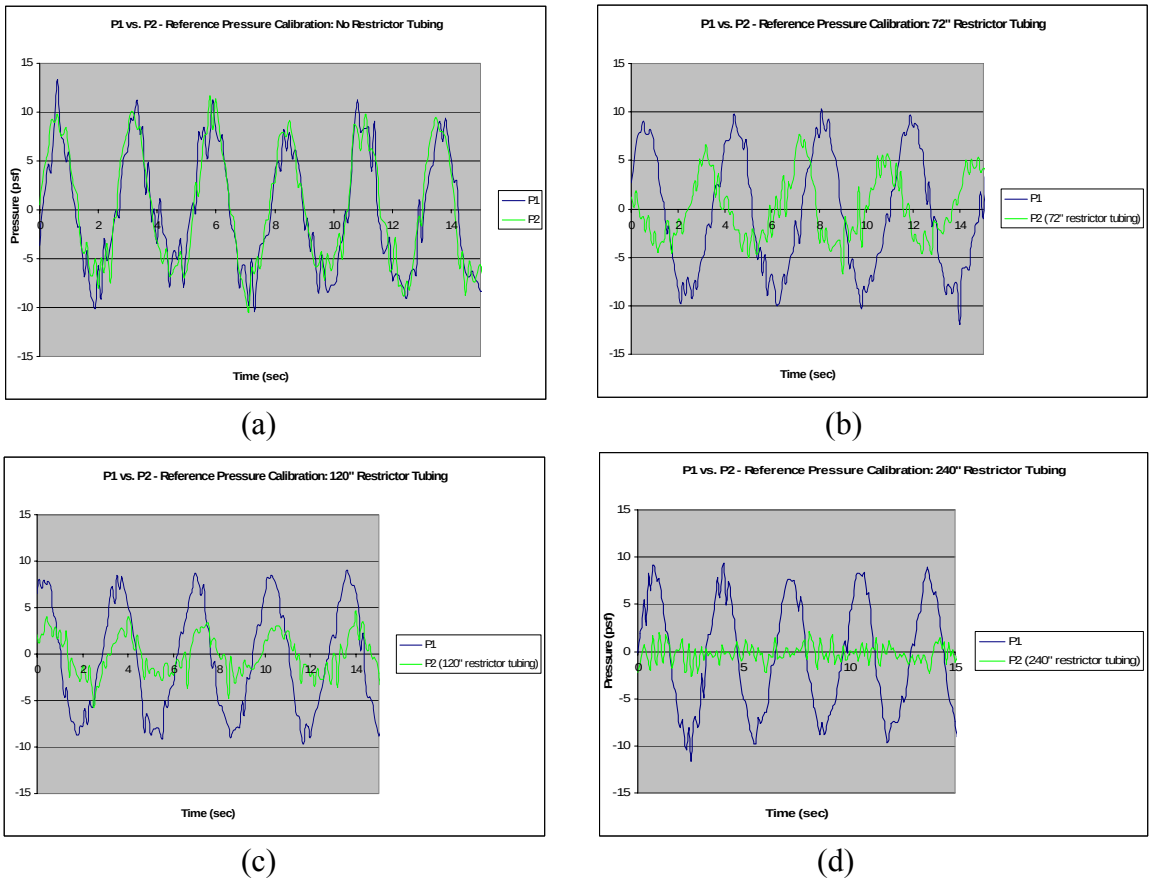

Figure 15. The Effect of Different Tubing Lengths on Pressure Time Histories, (a) Pressure Time Histories with no Restrictor Tubing, (b) Pressure Time Histories with No Tubing and with 72 in Restrictor Tubing, (c) Pressure Time Histories with No Tubing and 120 in Restrictor Tubing, (d) Pressure Time Histories with No Tubing and with 240 in Restrictor Tubing

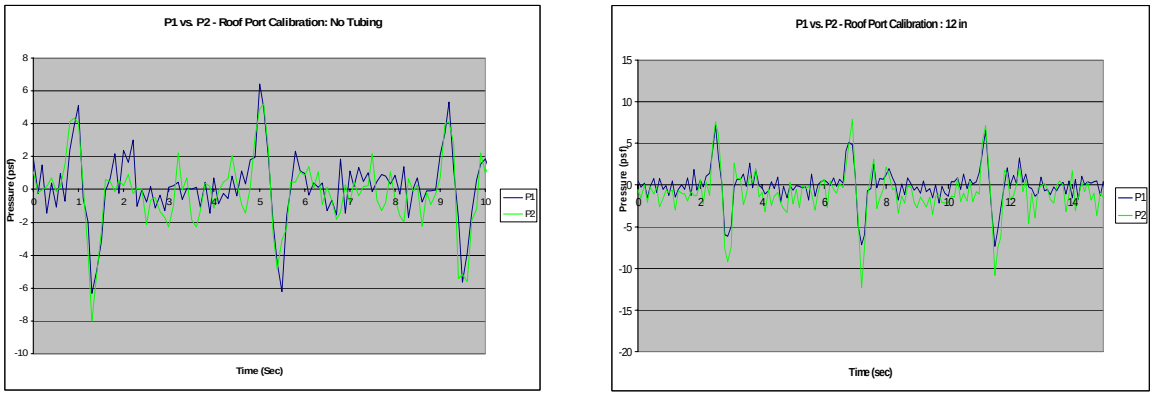

Figure 16. Roof Port Tubing Lengths, (a) Pressure Time Histories with No Tubing, (b) Pressure Time Histories with no Tubing and with 12 in ¼ in ID Polyurethane Tubing

The Free-Stream Velocity Profile

The first step in achieving the free-stream velocity profile measurements was to construct a moveable frame where wind monitors could be secured to take measurements. A frame was built using Unistrut, a system of galvanized steel beams, and connected together using grade A steel bolts (Figure 17). The steel frame measured 24 ft wide by 16 ft high and had a depth of 9 ft. Four wind monitors were secured to the frame in a square configuration with 8 ft sides (Figure 18), a configuration chosen so that the velocities of four fans could be measured simultaneously at the same reference point. This concept was very important to establish how the fans affected each other.

Figure 17. Unistrut Velocity Measuring Frame in Front of WOW

Figure 18. Close-up of Wind Monitor Frame Equipped with Four Wind Monitors

The Unistrut frame housing the wind monitors was able to move in three planes of motion via a system of sliding trolleys, pulleys and winches (Figure 19). Two electrically controlled winches controlled the side-to-side and up-and-down movement while movement toward and away from the diffuser was done by rolling trolleys. The winches made it possible to control the movement of the frame accurately from a safe distance from the WOW during testing. The external frame control system allowed for more exact placement of measurements, more efficient running of the engines and increased safety of the researchers.

After the frame was created to take velocity measurements and positioned a distance of 9 ft from the edge of the diffuser, the maximum velocity produced by the WOW running at 3000 rpm was determined. This wind speed was obtained through a series of trial and error tests where wind monitors where moved to several different locations to determine the position and value of the maximum wind speed. The

instantaneous peak wind speed achieved when the all 6 engines ran at 3000 rpm was 71 mph, representing a very strong tropical storm on the Saffir-Simpson hurricane intensity scale. At the time of this testing, the WOW was limited to running at a maximum 3000 rpm due to a carburetor problem which did not allow enough fuel to flow through the engine. As a result, after running the engines for a period of several minutes at a higher rpm, the engines would overheat and the pistons would melt. This problem was resolved with the help of new carburetors and larger fuel lines. After both scour and pressure testing were concluded, a second round of scour tests were conducted at the adjusted maximum of 4400 rpm. Additional velocity measurements were also taken and determined that the maximum wind speed at 4400 rpm was 129 mph, representing a strong Category 3 storm on the Saffir-Simpson scale.

Figure 19. Close-up Winch used to Move Unistrut Frame Up and Down and Side-to-Side

Once the maximum velocity at eave height was determined, the free-stream reference velocity profile along the span of the eave was measured. First, the frame was moved using the system described above, a distance of 6 ft from the edge of the diffuser

section. Velocity measurements, with a one-minute averaging time, spanning a 15 ft length at the eave height of the building were taken with all six fans running at 3000 rpm and again later at 4400 rpm. Another set of velocity measurements were taken at 9 ft from the diffuser section which represented the distance from the corner of the building to the diffuser section.

The determination of the maximum wind speed led way to a second round of measurements relating fan rpm to wind speed, necessary for gravel scour testing. Again, the Unistrut wind monitor frame was used, however, for the purpose of these measurements, the frame was fixed at the position where the eave height of the structure would sit as this was the area most crucial for the gravel scour testing and pressure testing.

All engines were first brought to their respective idle rpm for a brief warm-up period. The rpm of each engine was slowly increased, via the servo control, a small percentage while the wind monitors recorded velocities. Each time a velocity was recorded, the configuration of engines with their respective rpm was noted. After wind speed measurements were complete, curves were created for each individual engine reflecting the relationship between rpm and wind speed. These curves were used for gravel scour testing to determine the wind speed where gravel began scouring as wind speed measurements were not taken during actual testing.

Control Pressure Measurements

After initial velocity profiles were taken, the test structure was placed in front of the WOW and instrumented with pressure transducers so that control pressure

measurements could be taken for the pressure testing. Using the curve relating rpm and wind speed, six-min pressure time histories were recorded while all engines of the WOW ran at 3000 rpm. As mentioned previously, this rpm corresponded to a maximum wind speed of 71 mph. Measurements were taken with the test structure positioned at a 45° angle with respect to the WOW without any type of edge shape attached. These pressure values were later used to determine reductions in uplift on the roof with the presence of the modified edge shapes.

4. Experiments

This study consisted of two different tests which aimed to help better understand the development of vortices through visual testing and better protect against damage caused by vortex generation through product testing. This chapter will outline the specific test procedures for both tests.

Experimental Test Shapes

A total of four modified edge shapes and two standard edge shapes were tested between the gravel scour testing and the pressure testing. The modified edge shapes were designed and patented by Jason Lin Ph.D., Vice President of Weather Predict Consulting Inc. under the AeroEdge™ trademark. AeroEdge™ represents a family of patented aerodynamic devices, to be installed on roof and wall edges to suppress force-generating edge vortices. Products are non-intrusive exterior devices representing a simple and inexpensive way to equip new construction as well as retrofit existing construction. The four modified shapes used were the Flat-Roof AeroEdge™ Cap (patented), the Flat Roof AeroEdge™ Guard (patent pending), the Gable Edge Cap Vortex Suppressor (patented) and the Gable Edge Screen Vortex Suppressor (patent pending)(Figure 20).

The gable edge shapes were slightly modified in their application to the flat roof to account for the different slope of the roof and both shapes were similar in design to their flat roof counterparts with the exception of their height which was generally much shorter. The testing of the gable edge shapes mainly contributed to determining a relationship between edge shape height and the degree to which suction was reduced as

previous tests have suggested that shorter edge shapes are not as effective in mitigating roof suction.

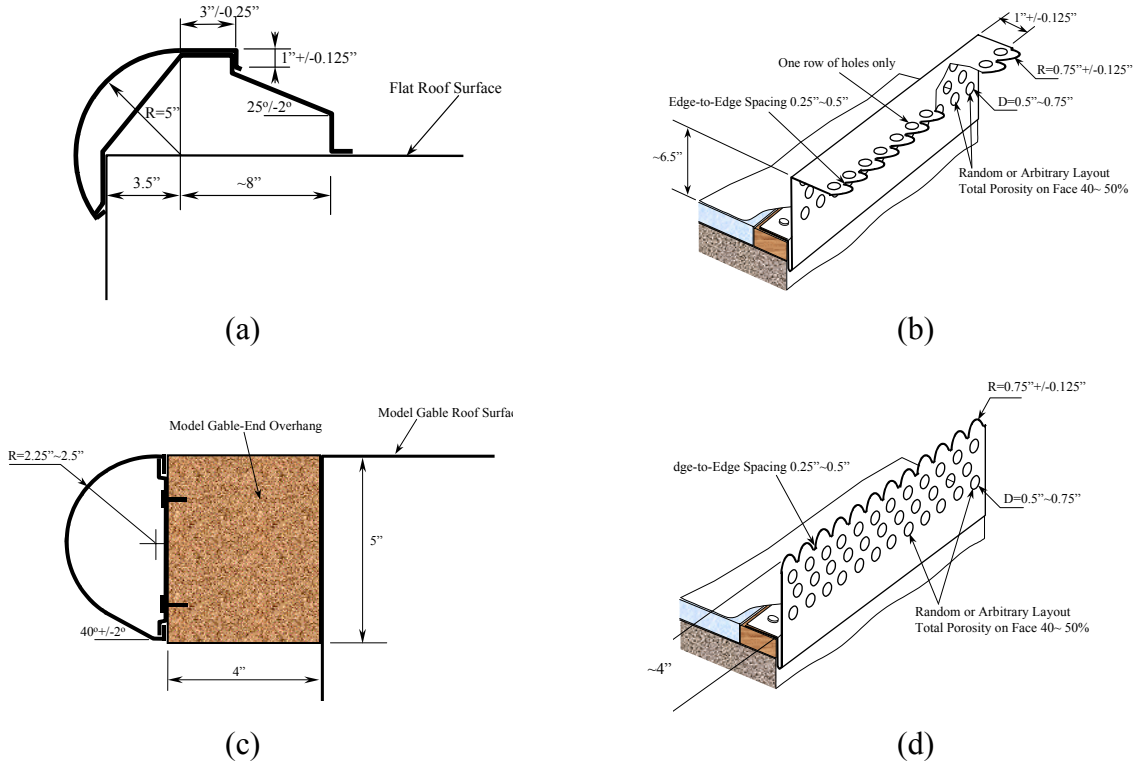

Figure 20. Modified Edge Shape Designs, (a) Flat Roof AeroEdge Cap, (b) Flat Roof AeroEdge Guard, (c) Gable Roof Edge Cap Vortex Suppressor, (d) Gable Edge Screen Vortex Suppressor

Surry and Lin (1995) described several aerodynamic mechanisms through which roof suction could be reduced through modified edge shapes. These aerodynamic mechanisms are reflected in the design of the AeroEdge^{TM} products and include the following:

(1) Eliminating sharp edges that create vortices

(2) Disrupting the vortices formation

(3) Disturbing the vortices

(4) Displacing the formed vortices

The remaining two edge shapes tested, which are currently prescribed in construction, were the Econosnap standard edge fascia and the Drain-Thru Gravel Stop (Figure 21). Because these shapes are an industry standard, pressure data representative of what an actual flat roof structure would feel during a storm was collected. All of the above products were manufactured by the Hickman Company, located in Asheville, NC.

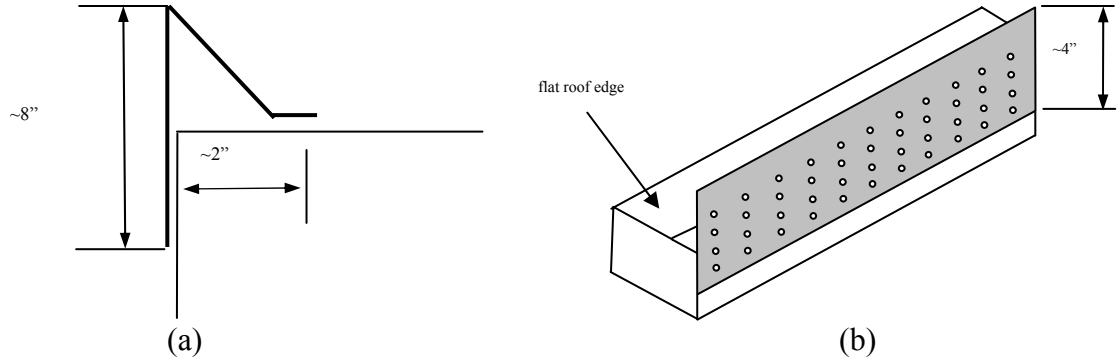

Figure 21. Standard Edge Shape Designs, (a) Econosnap Standard Fascia, (b) Drain-Thru Gravel Stop

Experiment 1 – Gravel Scour Testing

The first experiment done for this study was the gravel scour testing. This test focused on understanding the visual concept of vortex generation while also examining the affects of vortex suppression methods on the physical structure of the vortex. Four different edge shapes were tested including the standard Econosnap Fascia, the Drain-Thru Gravel Stop, the Flat Roof AeroEdge Cap, and the Flat Roof AeroEdge Guard. A professional photographer positioned on a platform above the WOW captured footage of all testing. The platform was located a safe distance from the WOW and allowed for a clear view of the roof top at a down-looking angle of 30°.

For the first test configuration in this series, the test structure, equipped with the standard Econosnap Fascia on the windward side and a 4 in porous parapet on the leeward side, was placed in front of the WOW at a 45° angle with respect to the WOW (Figure 22). The porous parapet was present on the leeward side of the structure for all testing, and in this case, was used as a mechanism to keep large amounts of gravel from spilling of the roof. The roof was then covered with a 2 in thick layer of ¼ in nominal diameter river gravel. All six engines of the WOW were brought to idle speed and then rpm was gradually increased until the gravel on the roof began to scour. Once the gravel scour commenced, the engines were brought back down to idle.

Figure 22. Test Structure Equipped with Econosnap Standard Fascia

Gravel scour was observed at 2750 rpm for this configuration which corresponded to a 60 mph maximum wind speed. A waveform was then created to reflect this transition point. The waveform first brought the engines up to the critical 2750 rpm where they were held for two minutes. The rpm was then increased to 2800 rpm for two minutes, 2900 rpm for another two minutes then 3000 rpm for a final three minutes

making the test duration a total of nine minutes (Figure 23). A series of digital photos were taken after this test and each subsequent test was completed to document the shape and size of the scour.

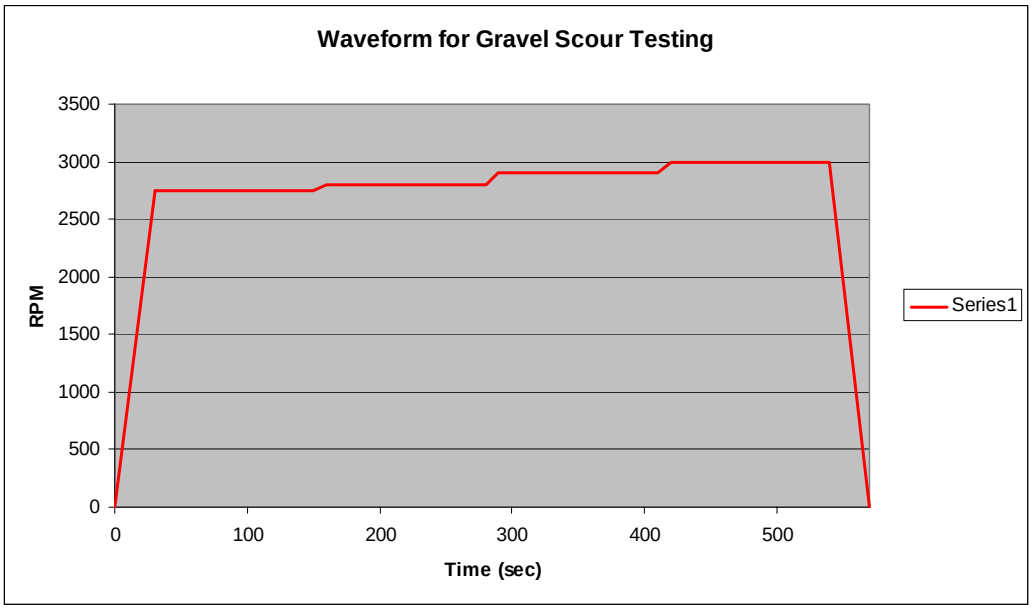

Figure 23. Waveform Function for Standard Edge Shapes, Econosnap Fascia and Drain-Thru Gravel Stop for Gravel Scour Testing

For the second test configuration, the standard Econosnap Fascia was replaced by the Standard Gravel Stop on the windward side of the structure (Figure 24). A 2 in thick layer of ¼ in nominal diameter river gravel was replaced on the roof. All six engines were turned on and brought up to idle rpm. The engine rpm was again brought gradually upward until visible movement of gravel was noted. Similar to the previous test, visible movement of gravel was observed at 2750 rpm or 60 mph. The same waveform run in the first configuration was run again for a nine minute duration during which time video footage captured the evolution of the gravel scour.

For the third configuration, the Drain-thru Gravel Stop was replaced by the Flat-Roof AeroEdge Guard (FRAG1) (Figure 25). The roof surface was refilled with a 2 in

layer of ¼ in thick nominal diameter river gravel. The WOW was then run using the same procedure as the previous test where the engines were brought to idle and then increased until scouring was observed. Because of the altered configuration of the test structure, only slight gravel scour was observed at the maximum 3000 rpm. To account for this difference in rpm, a new waveform was created starting the engines at idle rpm and ramping engines to 3000 rpm for seven minutes. Video footage was recorded simultaneously as the waveform was run.

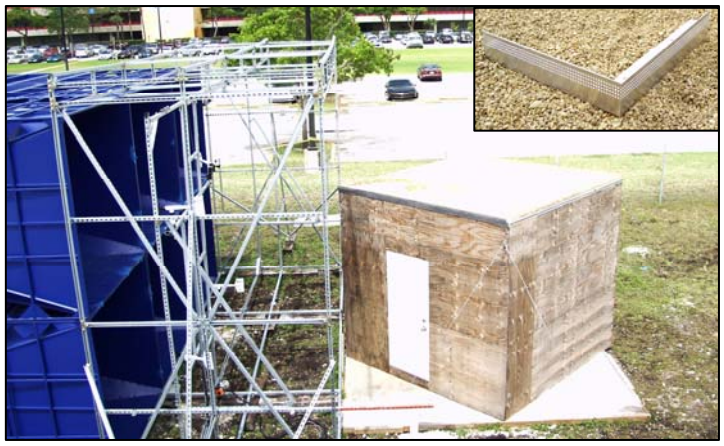

Figure 24. Test Structure Equipped with Drain-Thru Gravel Stop

Figure 25. Test Structure Equipped with Flat Roof AeroEdge Guard

For the fourth and final test configuration, the FRAG1 was replaced by the Flat Roof AeroEdge Cap (FRAC1) on the windward side of the structure (Figure 26). A run of the engines from idle to maximum rpm again indicated only slight gravel scour at 3000 rpm. The same waveform run for FRAG1 testing was run again while video was recorded.

Figure 26. Test Structure Equipped with Flat Roof AeroEdge Cap

Experiment 2 – Pressure Testing to Evaluate Vortex Suppression

The next set of tests served to establish the influence of vortex mitigation techniques in reducing suction pressures under the influence of the wind speeds produced by the WOW. For these tests, the same test structure was used and was situated in front of the WOW at a 45° angle. Simultaneous pressure measurements were taken throughout this experiment. Sixteen pressure taps were installed on the roof in a triangular configuration with the majority of taps concentrated in the Zone 3 roof zone as defined by ASCE 7-05 (Figure 27). According to ASCE 7-05, the Zone 3 area represents the

section of the roof that will experience the worst suction pressures and therefore has the most strict design criteria. The area is calculated based on the critical distance "a" which is the smaller value of 10% of the least horizontal distance of the structure or 0.4h (where h=height of the structure); this value cannot, however, be less than 4% of the least horizontal dimension or 3ft. Based upon the dimensions of the structure to be modeled, the critical distance "a" is calculated to be 3 ft resulting in an effective Zone 3 wind area of 9 ft^2. It was crucial to have the taps concentrated in this area in order to properly record the fluctuating pressures in that section of the roof.

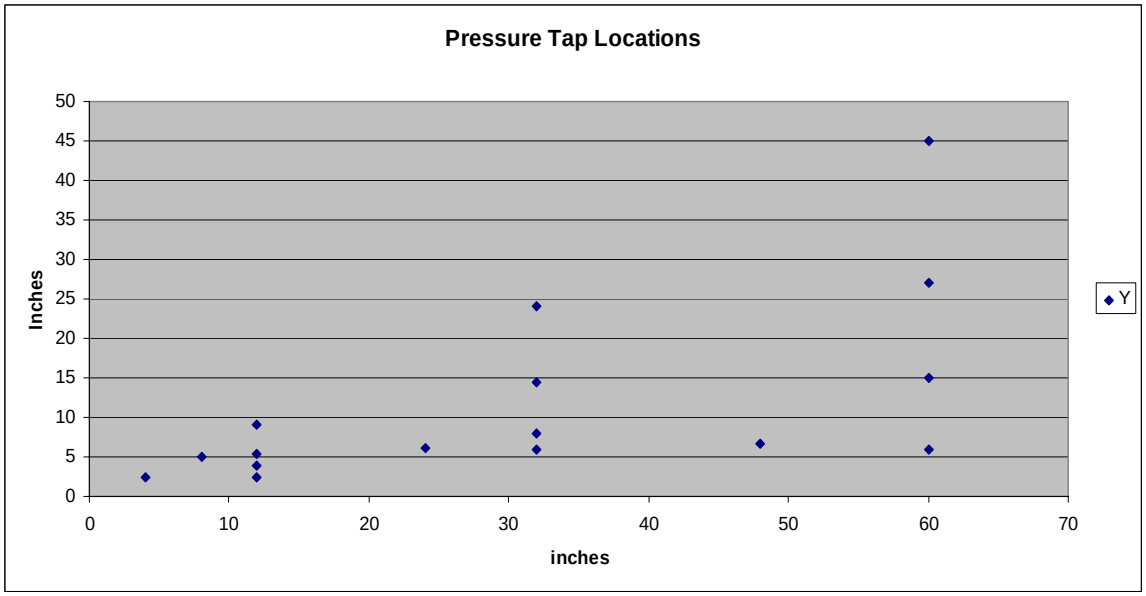

Figure 27. Pressure Tap Locations with Coordinate (0,0) referencing the roof corner and the horizontal and vertical axis representing the x and y axis respectively.

Table 1. X and Y Coordinates of Pressure Tap Locations

	X	Y
P1	4	2.5
P2	8	5
P3	12	2.375
P4	12	3.8125
P5	12	5.4375
P6	12	9
P7	24	6.125
P8	32	6
P9	32	8
P10	32	14.375
P11	32	24
P12	48	6.75
P13	60	6
P14	60	15
P15	60	27
P16	60	45

Seven different edge configurations, including a control test, were tested to determine their effects on reducing suction caused by conical vortices. The different configurations are described below.

Configuration1: Test Structure with no edge shape attached (control test).

Configuration 2: Standard Econosnap Fascia on the windward side of the structure and Gable Edge Screen Vortex Suppressor on the leeward side.

Configuration 3: Standard Drain-Thru Gravel Stop on the windward side of the structure and Gable Edge Screen Vortex Suppressor on the leeward side

Configuration 4: Flat Roof AeroEdge Guard on the windward side of the structure and Gable Edge Screen Vortex Suppressor on the leeward side.

Configuration 5: Gable Edge Vortex Cap Suppressor extended 2.375 in above the roof surface on the windward side of the structure and Gable Edge Screen Vortex Suppressor on the leeward side.

Configuration 6: Gable Edge Vortex Cap Suppressor extended .5 in above the roof structure on the windward side of the structure and Gable Edge Screen Vortex Suppressor on the leeward side.

Configuration 7: Gable Edge Screen Vortex Suppressor on both the windward and leeward sides of the structure.

A standard test procedure was employed for each of the seven tests. First, the edge shape being tested was installed on the roof using 1 ¼ in galvanized ring shank nails, the standard fastener used to install edge fascia in current building practices. Next, a wave form was created which brought the engines from idle rpm to 3000 rpm for six minutes and then back down to idle (Figure 28). This waveform was chosen to fulfill two main objectives of this study. First, it was essential to collect full-scale pressure data under worst-case tropical cyclone conditions. By running the engines at 3000 rpm, it was possible to recreate tropical storm conditions in the full-scale environment and collect corresponding pressure data. Second, because gravel scour testing was also tested at 3000 rpm, a comparison could be made regarding the area where gravel scour occurred and the corresponding pressures. This wave form was run for each different edge configuration.

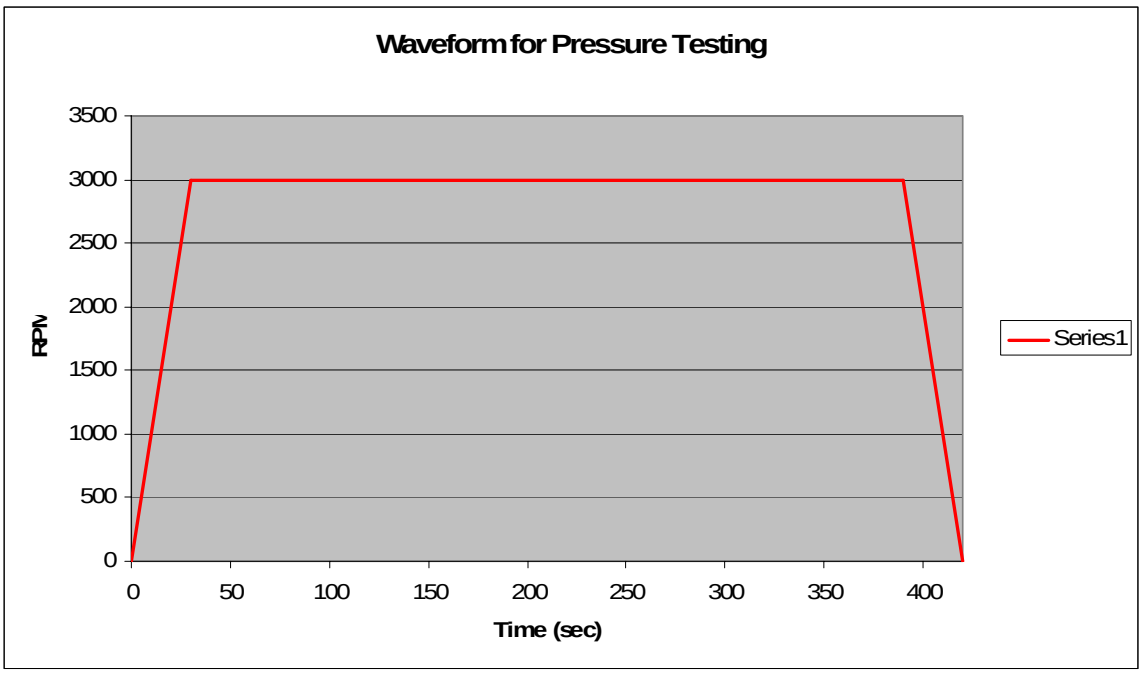

Figure 28. Waveform used to run Engines for Pressure Testing

Pressure data was collected simultaneously while the waveform was run. All transducers sampled data at 100 Hz for six minutes. The seven resulting time histories were then transferred from the DAQ for data analysis.

Experiment 3 – Gravel Scour Testing at 4400 rpm

After initial gravel scour testing and pressure testing were completed, a second round of gravel scour testing was performed at the maximum 4400 rpm. For the second round of tests only the standard Econosnap Fascia and FRAG1 edge shapes were tested as the other two edge shapes resulted in similar gravel scour patterns. The shapes were installed in the same manor as in the previous gravel scour testing and the tests structure was again positioned at 45° with respect to the WOW.A waveform was created which brought the WOW from idle rpm to 4400 rpm in 30 seconds for a duration of one minute.

This waveform was run three times so that the test structure was subjected to 4400 rpm or 129 mph maximum wind speeds for three minutes, though not consecutively (Figure 29).

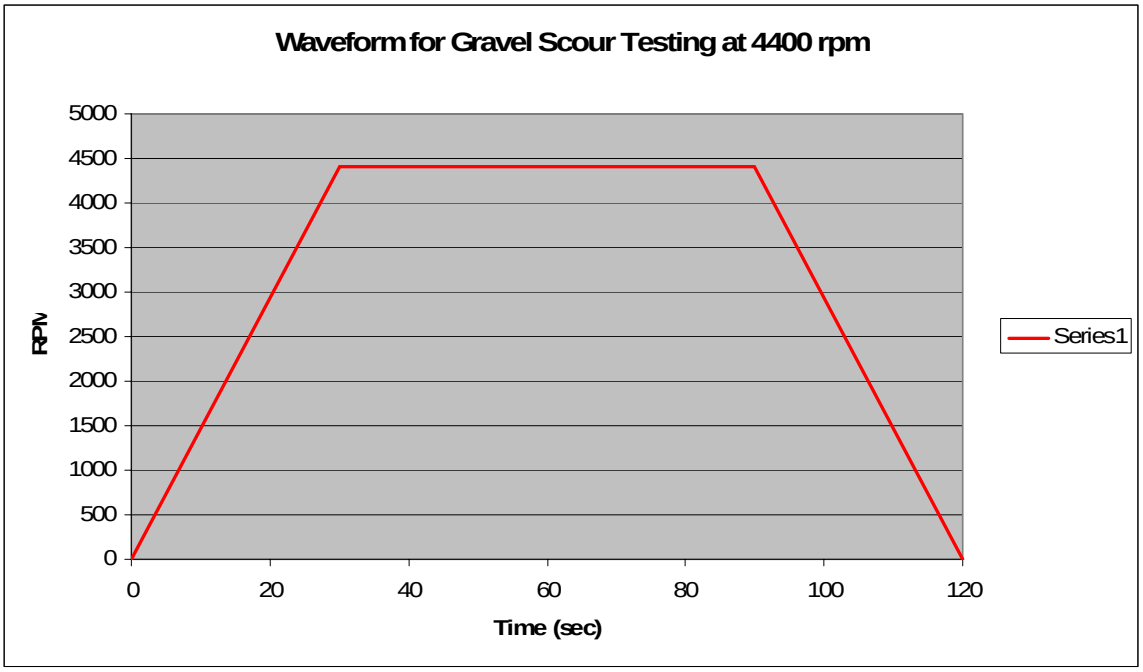

Figure 29. Waveform for Second Round of Gravel Scour Testing

Data Analysis

Data analysis for the gravel scour tests involved qualitative and quantitative analysis of digital photos to observe how modified edge shapes affected the visual structure of the vortex. This evaluation made it possible to determine whether or not a particular edge shape was effective in vortex suppression. All images were compared back to the standard roof which consisted of a gravel roof equipped with the Econosnap Fascia.

Three different criteria were used to evaluate images and determine whether or not a particular modified edge shape could potentially reduce suction pressures. The first

criterion involved comparing the wind speeds at which gravel scour was first observed. If a modified edge shape increased the wind speed where gravel scour began it was considered potentially effective in reducing suction caused by cornering winds.

Next, the magnitude of gravel scour was considered. Previous studies have shown that modified edge shapes both reduce the suction at the windward corners and cause a more uniform pressure distribution so that the entire roof is under the same reduced amount of force. This reduction would appear visually if the size of the area affected by gravel scour was reduced with the presence of a modified edge shape. To achieve this comparison, dimensions of gravel scour area were taken after each test so that a comparison could be made to the standard roof and the shape could be evaluated for effectiveness. If gravel scour area at the roof corner was decreased and the roof displayed a uniform gravel scour over the majority of the remaining roof section, the shape was considered potentially effective in vortex suppression.

The final criterion to be considered was the location where gravel scour was initiated on the roof. Modified edge shapes have often had the effect of deflecting turbulent flow vertically above the structure and horizontally away from the corner regions. Deflecting the flow horizontally is considered advantageous as it both reduces suctions caused by the vortices and causes any additional suction to occur away from the essential connections which secure the roof to the structure. If the presence of an edge shape was able to influence the location of the initiation of gravel scour, it was considered likely that that same edge shape would result in decreased suction pressures.

After a visual analysis of gravel scour was concluded, pressure time histories were analyzed to determine the quantitative reduction in suction pressures caused by

modified edge shapes. In order to analyze this data, differential pressure values obtained during pressure testing were first converted to pressure coefficients. Pressure coefficients are dimensionless quantities defined as the differential pressure divided by the dynamic pressure (Eq. 1). Pressure measurements were non-dimensionalized for comparison purposes. By performing this conversion, pressure coefficients from this study could be compared to quantities recorded in previous studies without having to consider similarities in wind speed.

$$C_p = \frac{\Delta p}{\frac{1}{2}\rho V^2} \qquad \text{(Eq. 1)}$$

where C_p is the pressure coefficient, ρ is the density of air, and V is velocity.

The velocity values used to non-dimensionalize were obtained from measurements taken during initial velocity measurements at the eave height. A curve of the mean velocity profile was created and the coordinates representing the location of the pressure taps were transposed to the plane of the velocity measurements (Figure 30). By representing the pressure tap locations on the plane of measurement, wind speeds specific to each tap could be used to calculate the dynamic pressure making pressure coefficients were more accurate.

The data analysis of the pressure time histories had 3 main objectives:

1. Compare time histories and determine whether or not a reduction in Zone 3 suction pressures occurred due to the aerodynamic edge shapes

2. Compare peak pressure from both control and aerodynamic edge shape testing to values suggested by ASCE 7-05 to determined whether or not more conservative values should be implemented
3. Establish co-relation of pressure values between different points of the roof to determine if aerodynamic edge shapes were effective in breaking the coherency of the shed vortices

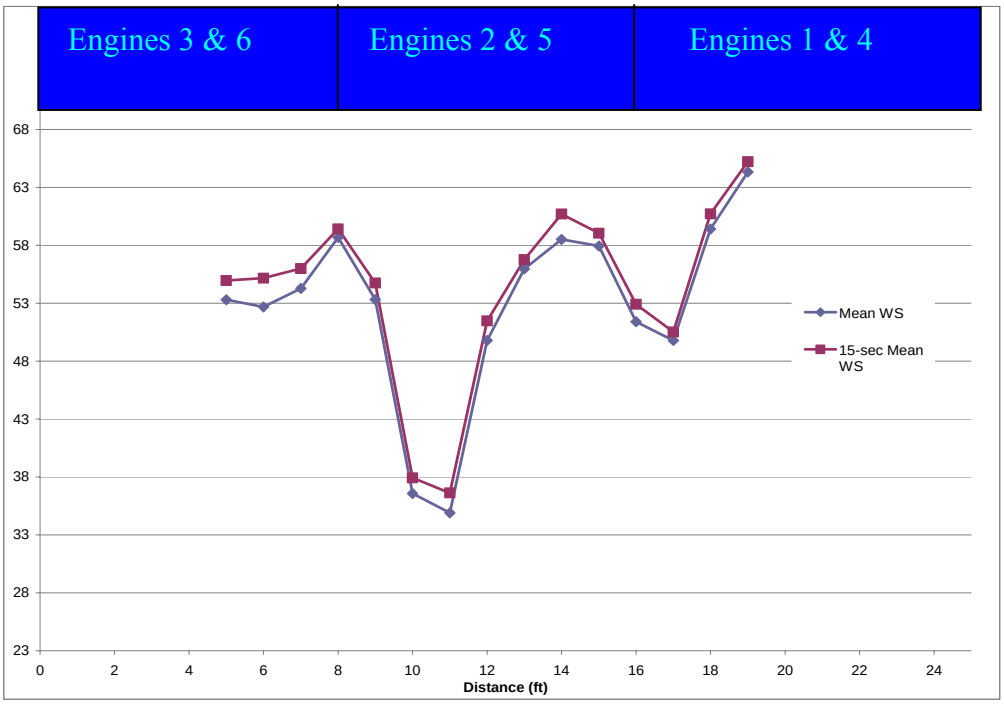

Figure 30. Wind Velocity Profile from WOW at 3000 rpm

The first objective was accomplished by recreating the pressure time histories using the pressure coefficients instead of the differential pressure values. Pressure coefficients were then used to calculate $C_{p\ min}$, $C_{p\ max}$, $C_{p\ mean}$, and $C_{p\ rms}$ for each tap and each different test. These values were compared to the values recorded for the control test and the percentage difference was calculated in order to evaluate the reduction in roof corner suction.

The $C_{p\ min}$ and $C_{p\ max}$ values obtained for the control test were then compared to ASCE 7-05 Zone 3 design coefficients to determine whether or not current code values are adequately conservative. This was done to verify that design values obtained from wind tunnel testing and modeling accurately describes what is actually occurring in the atmosphere. If design values are too conservative than structures can be over-designed resulting in unnecessary use of supplies and money. On the other hand, a structure not designed to code could suffer catastrophic damage in the event of a sever storm.

The $C_{p\ min}$ and $C_{p\ max}$ values obtained from pressure testing of modified edge shapes were also compared to current design values to determine if the addition of a modified edge shape would reduce suction enough that the Zone 3 region could actually be designed under Zone 2 values. This comparison would establish whether or not the presence of aerodynamic edge shapes would constitute the design of Zone 3 by Zone 2 values. As mentioned previously, a current provision in the code makes this exception for the presence of parapets that meet a certain height requirement.

Three-dimensional plots were created showing pressure data for each individual test to establish a co-relation of pressure values between different points on the roof. The control test with no modified edge shape was again used as a basis for comparison as the co-relation between points in this case would represent the common case for current structures. As concluded in previous studies and verified in this full-scale study, the case with no modified edge shape demonstrated extremely high suction on the corner and along the edge of structure which reduced drastically with distance from the edge. Three-dimensional plots from pressure testing with modified edge shapes were therefore not only examined for reduction but different pressure patterns altogether. One hypothesis of

this study was that the modified edge shapes may drastically reduce suction at the corner while having little effect on the slight suction seen towards the middle of the roof. This case would result in a more uniform pressure distribution and contour plots were evaluated for changes in co-relation such as this. Three-dimensional plots were also scanned for an appreciable increase in positive pressure anywhere on the roof which would essentially have the opposite effect of suction but still cause significant damage.

5. Results and Discussion

Gravel scour and pressure testing were conducted to evaluate the influence of modified edge shapes on the structure of conical vortices and roof corner suction pressures, respectively. Four different edge configurations were tested for gravel scour and seven for pressure testing. Results indicated that certain edge shapes did have an impact on both the structure of the conical vortices and the pressures experienced at the roof corner region.

Gravel Scour Testing Results

Gravel scour testing resulted in a noticeable difference between the scour occurring with the Econosnap Fascia and Drain-Thru Gravel Stop and that occurring with FRAG1 and FRAC1 AeroEdge^{TM} edge shapes. The Econosnap Fascia lead way to a significant area of gravel scour initiated at the roof corner (Figure 31). At its furthest point, the scour extended a distance of 42 in from the corner of the roof and spanned 19 in across at its widest point. A ray superimposed on the digital photos extending from the corner towards the middle of the roof at a 45° angle with respect to the roof edge acted as a center line in order to compare whether or not scour patterns were symmetrical. In this case, the centerline made it apparent that the pattern of scour was highly asymmetrical with significantly more scour occurring to right of the reference line, or the west side of the structure. From this observation it was concluded that the flow was slightly turbulent. The turbulent nature of the flow could be attributed to environmental cross winds, asymmetrical obstructions at the test site, or natural turbulence caused by the framing of the WOW. Though it is noteworthy to observe that turbulence does exist on the flow,

this study is primarily focused on the area affected by gravel scour and not necessarily the shape therefore it is not important to specifically classify these turbulence characteristics.

Figure 31. Gravel Scour Associated with the Econosnap Edge Fascia

The Drain-Thru Gravel stop also resulted in a significant amount of scour (Figure 32). Like the Econosnap Fascia, the scour initiated close to the corner of the roof, however, a small area of gravel right at the corner remained intact. The scour resulting from the Drain-Thru Gravel Stop was much more symmetrical than the previous pattern, forming a heart-shaped pattern nearly evenly distributed on either side of the superimposed centerline. The scour extended 39 in from the roof corner to the center of the roof along the centerline. The "peaks" on either side of the heart extended 42 in from the roof corner towards the center of the roof and at its widest point the heart shape measured 30 in. The scour pattern also illustrated the fact that the vortices formed at

about a 15° angle form the southeast and southwest edges of the structure. This is consistent with previous studies which have showed that conical vortices form on both edges adjacent to the leading corner at angles anywhere from 10-15°.

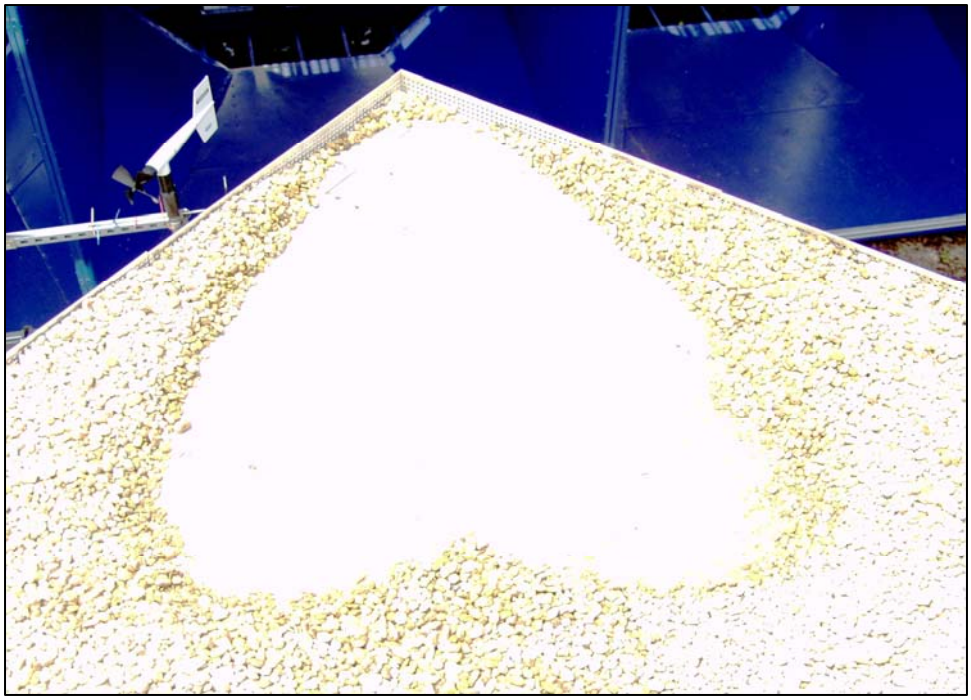

Figure 32. Gravel Scour Associated with Drain-Thru Gravel Stop

Both the FRAG1 and FRAC1 modified edge shapes appeared to have suppressed the suction associated with the conical vortices as no gravel scour was evident after the test took place (Figure 33, Figure 34). Digital photos and video taken during actual testing supported this assumption. Digital photos taken after running the waveform showed no obvious signs of scour and measurements taken after testing verified that the depth of the gravel remained the same at the corner both before and after the roof was subjected to tropical storm force winds. Video footage reviewed after the testing showed random gravel movement sporadically throughout the waveform; however, no significant

scour was observed. Results from these tests supplied visual support that the presence of modified edge shapes does affect the structure of the vortices. This change in vortex structure could be attributed to the vortex being deflected above the surface by the modified edge shape so it no longer interacted with the roof or the vortex being completely destroyed by the edge shape so that the flow pattern no longer existed.

Gravel scour testing at 4400 rpm revealed similar results to testing conducted at 3000 rpm. With the presence of the standard Econosnap Fascia, approximately ¾ of the roof surface experienced gravel scour in the same heart shape pattern seen at 3000 rpm (Figure 35). The FRAG1 edge shape again performed well by completely eliminating scour on the roof (Figure 36). Measurements recorded during pressure testing helped to determine how the change in the scour pattern corresponded to a change in roof pressure.

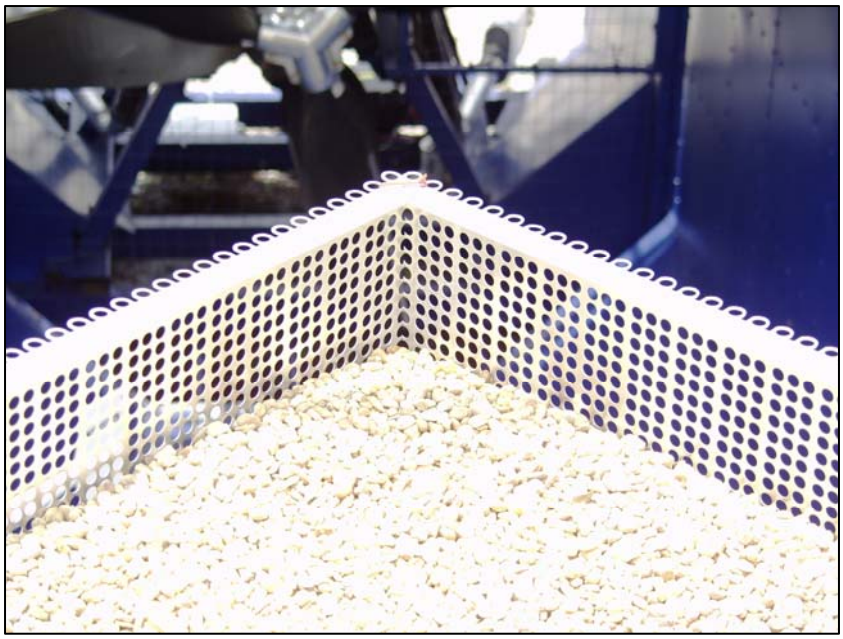

Figure 33. Gravel Scour Associated with FRAG1 AeroEdge™ Shape at 3000 rpm

Figure 34. Gravel Scour Associated with FRAC1 AeroEdge™ Shape at 3000 rpm

Figure 35. Gravel Scour Associated with Econosnap Fascia at 4400 rpm

Figure 36. Gravel Scour Associated with FRAG1 edge shape at 4400 rpm

Pressure Testing Results

Pressure testing results both verified the validity of the WOW in full-scale testing and revealed that the presence of certain modified edge shapes reduced the suction at the roof corner. Pressure data recorded during the control testing where no edge shape was attached to the roof was compared to similar data recorded from pressure taps 50001, 53001, 50044 and 53044, located at the four corners of the WERFL at TTU at wind angles of 45°, 135°, 225°, and 315°. A comparison between the data showed similarities in the magnitude of the $C_{p\ min}$ recorded at the four taps at TTU and values recorded at the taps closest to the corner during WOW testing. For example, WOW tap #3 recorded a $C_{p\ min}$ of -18.23 while the four TTU corner taps recorded $C_{p\ min}$ values around -20. The slight difference in values could be attributed to differences in environmental conditions, etc., however, the fact that data is so close given two completely different test methods is very promising for the future of the WOW. This conclusion is extremely important to the prospect of the WOW as it shows that the flow produced by the WOW is very similar to the atmospheric flow and thus it is a valid and accurate way to perform full-scale testing on both building components and entire structures.

Pressure testing of modified edge shapes demonstrated that certain edge shape configurations had a significant impact on not only the suction pressure at the roof corner but also on the pressure distribution on the roof. The first test performed which was the control test with no edge shape, yielded typical results with high suctions present at the corners and edges which reduced with distance from the edge of the structure. The most negative pressure that occurred was recorded at pressure tap #3, located 12 in from the roof corner in the x-direction and 2.375 in from the roof edge in the y-direction. This tap

was especially vulnerable to feeling extreme suction because it was located closer to the edge of the structure in the y-direction than any of the other taps. The resulting $C_{p\ min}$ was -18.23 which was not only consistent with TTU data but also with wind tunnel studies conducted by Surry and Lin (1995) which yielded a $C_{p\ min}$ of almost -18 at a corner tap for boundary layer flow equivalent to the environmental flow at TTU. All of the taps along edge of the test structure yielded $C_{p\ min}$ values from -6 to -17.

The Econosnap standard fascia resulted in a similar pressure distribution with a minimum $C_{p\ min}$ value of -14.42 at tap #7. The Econosnap fascia had the effect of slightly reducing the extreme suction in the taps at the very corner but as a result, remaining taps recorded lower negative peak pressures. The Drain-Thru Gravel Stop, which was tested directly after the Econosnap Fascia, in most cases resulted in a slight increase of $C_{p\ min}$.

The FRAG1 standard edge shape yielded the best results in terms of reducing the overall suction on roof as it reduced the suction experienced by 14 out of the 16 taps. The most extreme peak suction recorded at tap #3 was reduced by 74% and the $C_{p\ mean}$ at the same tap was reduced by 71%. Overall, the $C_{p\ min}$ was reduced anywhere from 15-74% depending on the location of the tap. The $C_{p\ mean}$ values were reduced anywhere from 25-70%, again depending on the tap location. The resulting pressure distribution was much uniform due the presence of this edge shape which can be seen in the 3D-plots (see Appendix A). The $C_{p\ min}$ for all taps during this test was -7.35 with the presence of the FRAG1 which was significantly high compared to the minimum values present in the additional time histories with the remaining shapes. The range of peak $C_{p\ min}$ was between -2.15 and -7.35 which demonstrated that the pressure distribution became much more uniform with the presence of this edge shape. It is though that the FRAG1 edge shape

acted in destroying the rotational flow of the vortices altogether thus making it extremely successful in reducing uplift.

The Gable Edge Vortex Cap Suppressor extending 2.375 in above the roof of the test structure consistently reduced roof uplift by 10-45% on all taps except for #15. Though the reductions with this shape were not as considerable as in the previous shapes, the shape proved consistent in that it helped to alleviate the structure of suction pressure throughout the entire surface of the roof and not just in taps located close to the edge. The variation of the shape extending only 0.5 in from the roof of the test structure performed very similar to its taller variation by reducing suction at all taps except for #15 which was located close to the center of the roof. Reductions of 7-56% were observed for the remaining taps which reflected even more significant reductions than the taller version. Changes in $C_{p\ mean}$ were far less consistent as some taps reflected an increase in $C_{p\ mean}$ while some reflected a decrease in $C_{p\ mean}$. In either case, the changes were relatively insignificant. Though this shape did result in a slight reduction in uplift, it is not suggested that it be applied to a flat roof for the purpose of uplift mitigation; what can be concluded from these results is that a taller shape is needed to appreciably reduce uplift on a flat roof.

The final shape tested, the Gable Edge Screen Vortex Suppressor, both increased and decreased pressures depending on the location of the taps. While previous shapes also caused increases in suction at certain taps, the increases were quite small comparatively. In this case, the presence of the Gable Edge Screen Vortex Suppressor actually caused an increase in suction of 107% at tap #8 located along the edge of the roof and resulted in a minimum C_p of approximately -13 which was very similar to the

Econosnap Fascia case. These results are consistent with previous studies which have shown that shorter parapets have a tendency to increase suction on the roof at certain locations. The one positive aspect of this shape was that it did slightly reduce the range of pressures felt by the roof so the pressure distribution over the roof was somewhat more uniform. Figure 37 illustrates how each tap was affected by each shape.

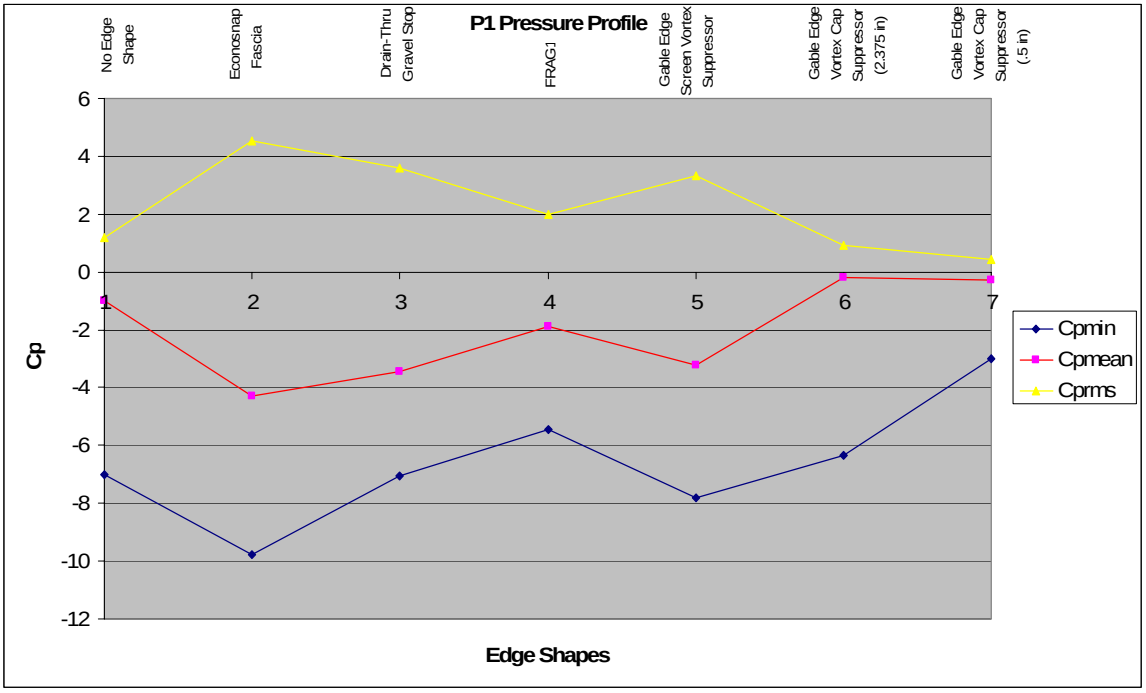
P1 Pressure Profile
No Edge Shape
Econosnap Fascia
Drain-Thru Gravel Stop
FRAG1
Gable Edge Screen Vortex Suppressor
Gable Edge Vortex Cap Suppressor (2.375 in)
Gable Edge Vortex Cap Suppressor (.5 in)
Cp
Edge Shapes
Cpmin
Cpmean
Cprms

(a)

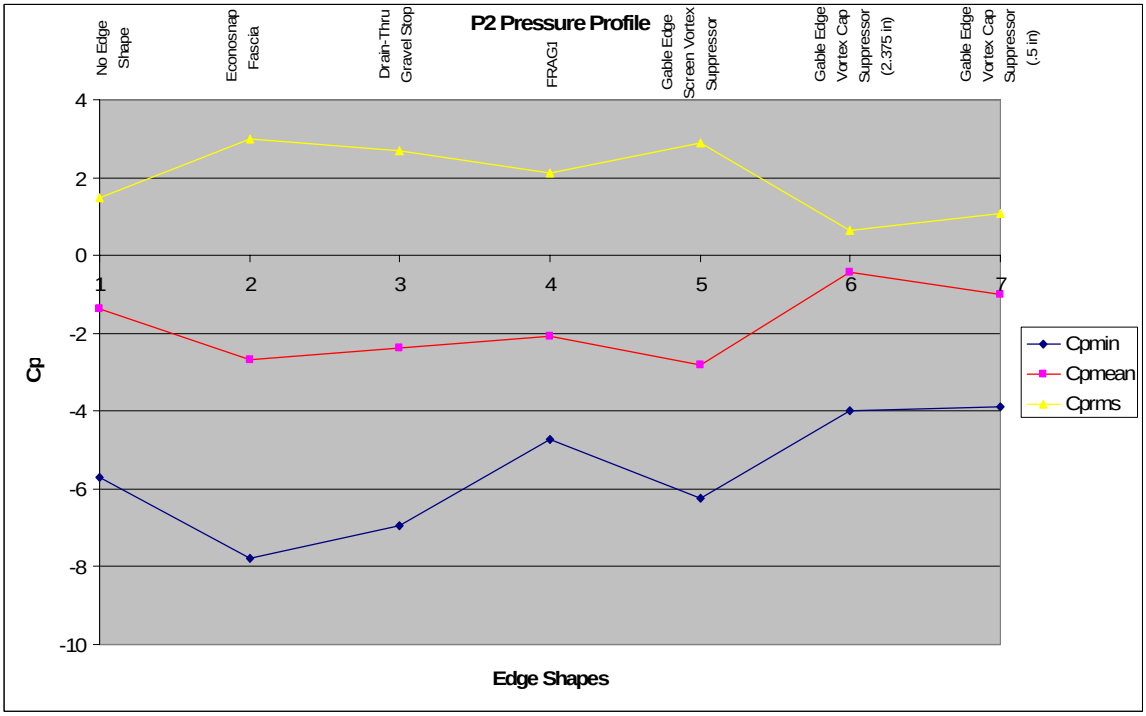
P2 Pressure Profile
No Edge Shape
Econosnap Fascia
Drain-Thru Gravel Stop
FRAG1
Gable Edge Screen Vortex Suppressor
Gable Edge Vortex Cap Suppressor (2.375 in)
Gable Edge Vortex Cap Suppressor (.5 in)
Cp
Edge Shapes
Cpmin
Cpmean
Cprms

(b)

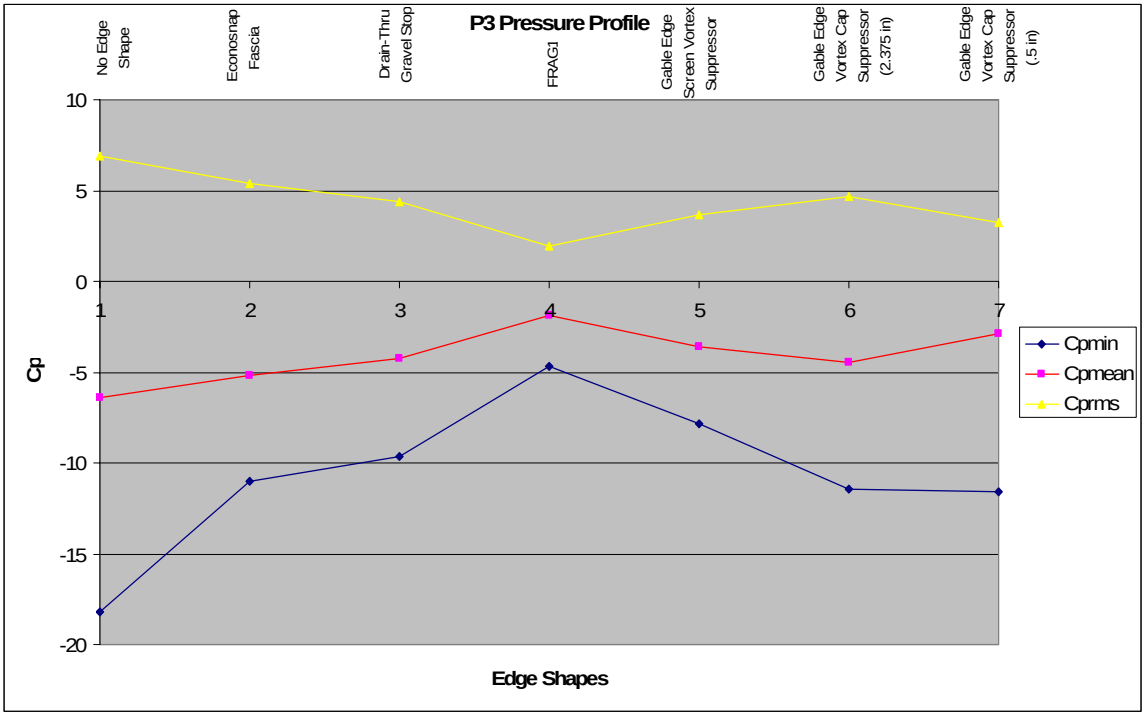
P3 Pressure Profile
No Edge Shape
Econosnap Fascia
Drain-Thru Gravel Stop
FRAG1
Gable Edge Screen Vortex Suppressor
Gable Edge Vortex Cap Suppressor (2.375 in)
Gable Edge Vortex Cap Suppressor (.5 in)
10
5
0
-5
-10
-15
-20
1
2
3
4
5
6
7
Cp
Cpmin
Cpmean
Cprms
Edge Shapes

(c)

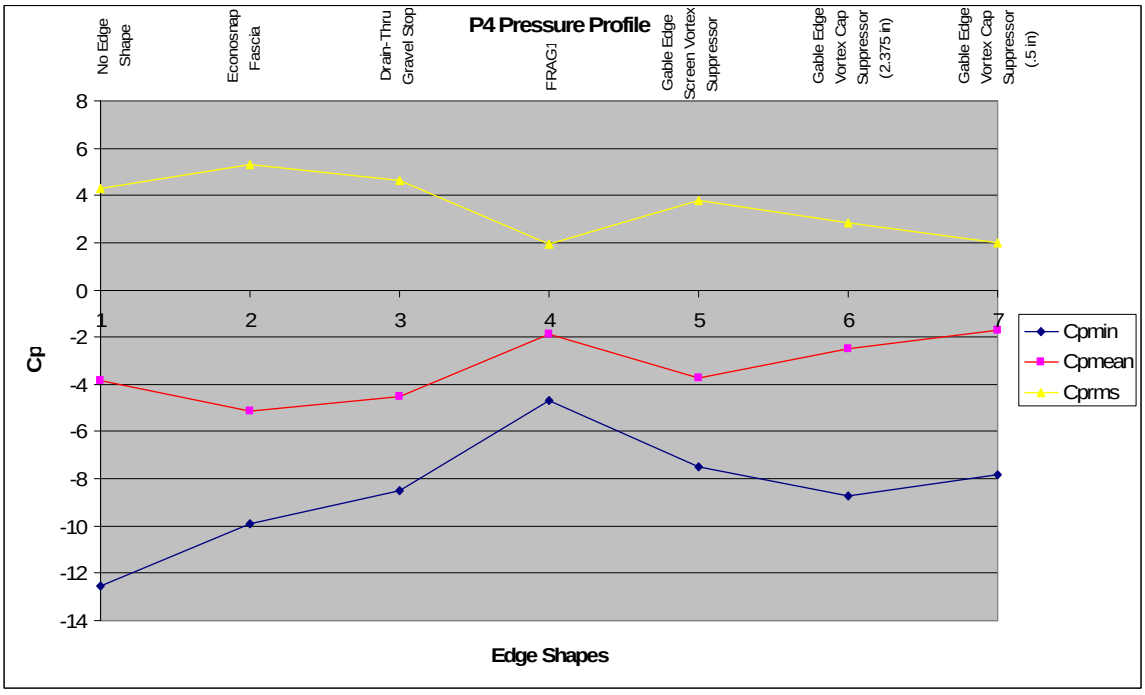
P4 Pressure Profile
No Edge Shape
Econosnap Fascia
Drain-Thru Gravel Stop
FRAG1
Gable Edge Screen Vortex Suppressor
Gable Edge Vortex Cap Suppressor (2.375 in)
Gable Edge Vortex Cap Suppressor (.5 in)
8
6
4
2
0
-2
-4
-6
-8
-10
-12
-14
1
2
3
4
5
6
7
Cp
Cpmin
Cpmean
Cprms
Edge Shapes

(d)

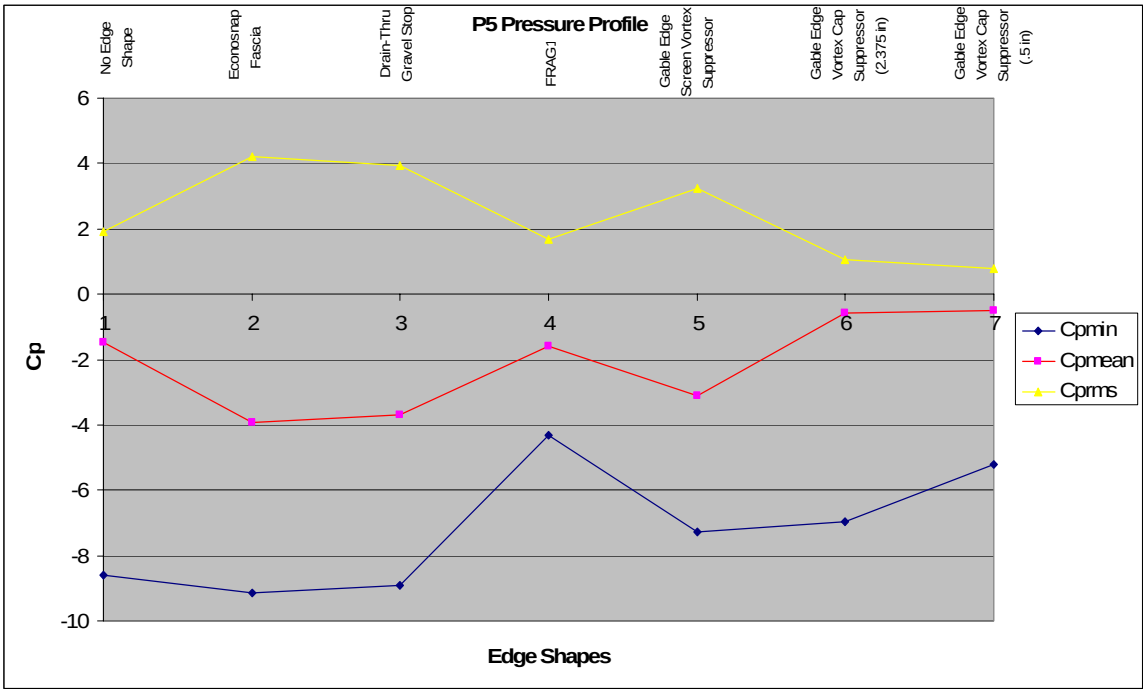
P5 Pressure Profile
No Edge Shape
Econosnap Fascia
Drain-Thru Gravel Stop
FRAG1
Gable Edge Screen Vortex Suppressor
Gable Edge Vortex Cap Suppressor (2.375 in)
Gable Edge Vortex Cap Suppressor (.5 in)
Cp
Edge Shapes
Cpmin
Cpmean
Cprms

(e)

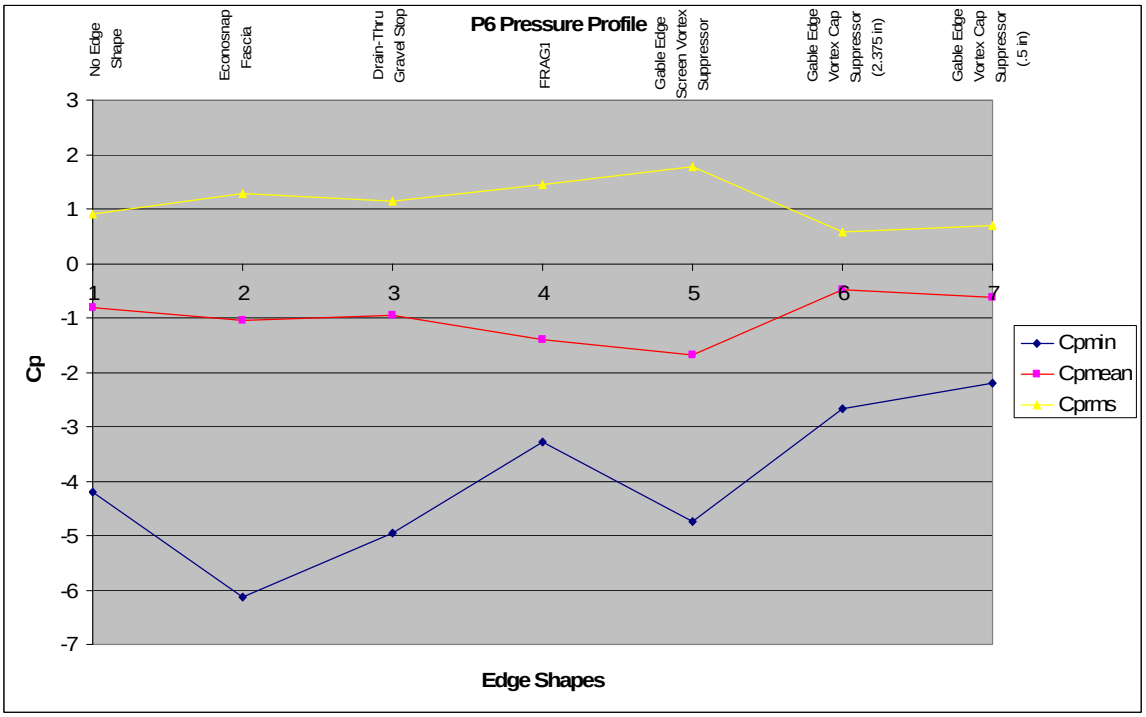
P6 Pressure Profile
No Edge Shape
Econosnap Fascia
Drain-Thru Gravel Stop
FRAG1
Gable Edge Screen Vortex Suppressor
Gable Edge Vortex Cap Suppressor (2.375 in)
Gable Edge Vortex Cap Suppressor (.5 in)
Cp
Edge Shapes
Cpmin
Cpmean
Cprms

(f)

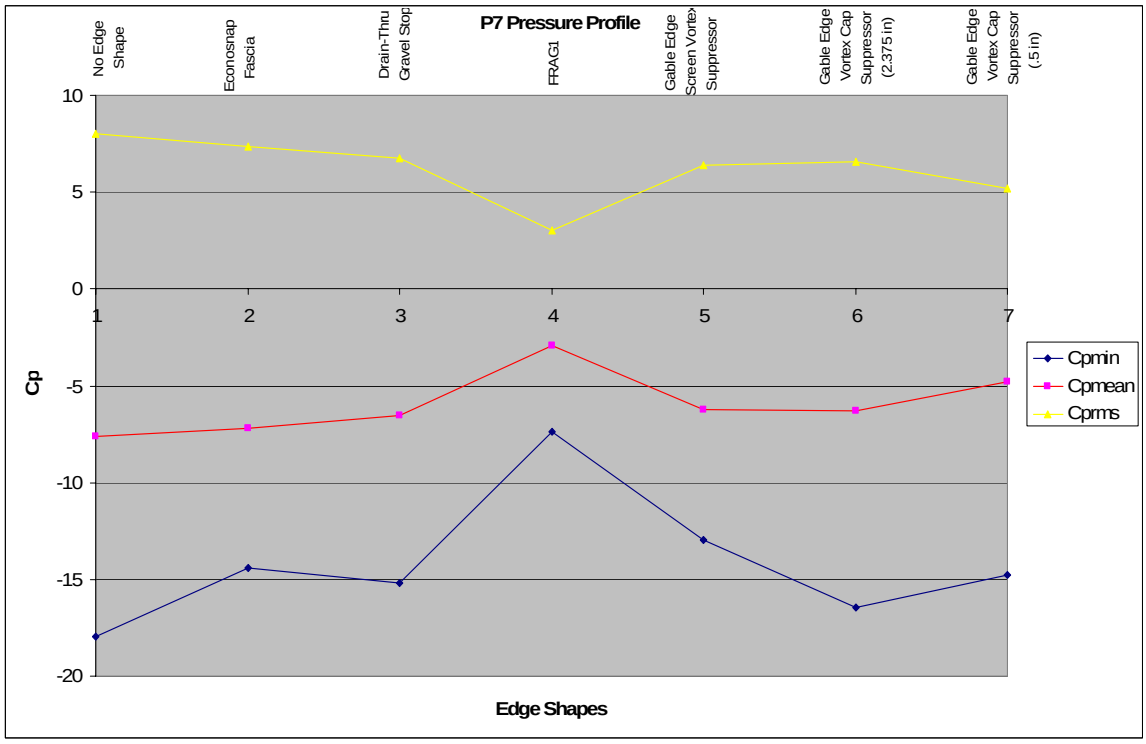
P7 Pressure Profile
No Edge Shape
Econosnap Fascia
Drain-Thru Gravel Stop
FRAG1
Gable Edge Screen Vortex Suppressor
Gable Edge Vortex Cap Suppressor (2.375 in)
Gable Edge Vortex Cap Suppressor (.5 in)
10
5
0
-5
-10
-15
-20
1
2
3
4
5
6
7
Cp
Cpmin
Cpmean
Cprms
Edge Shapes

(g)

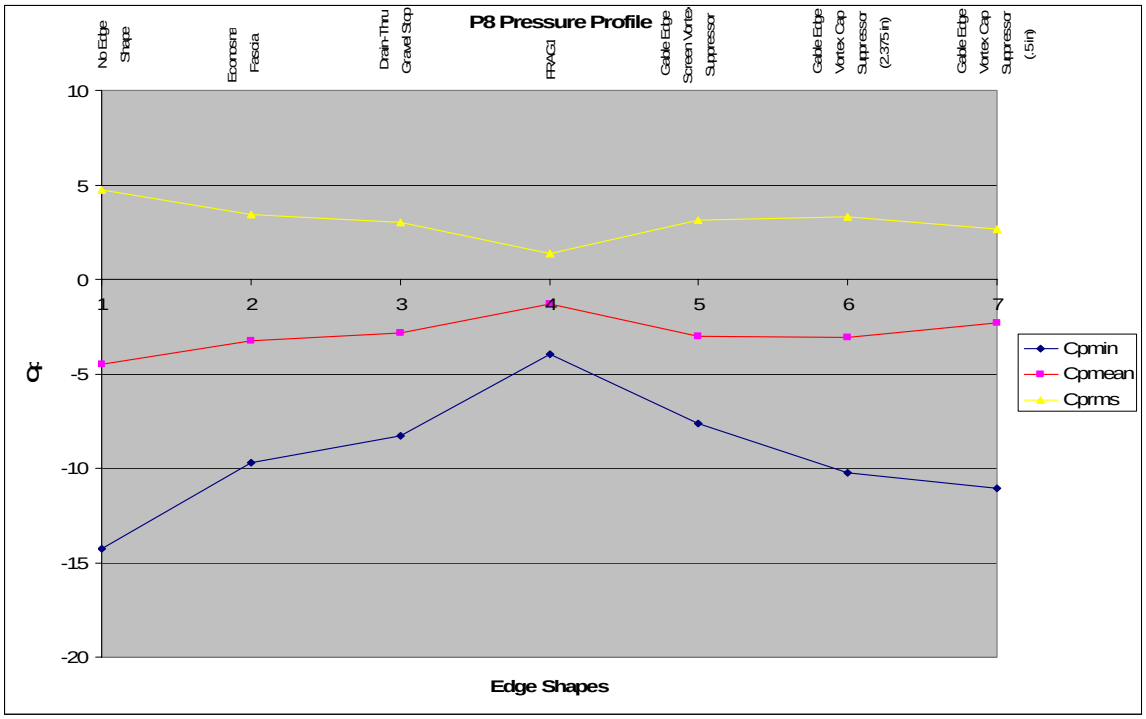
P8 Pressure Profile
No Edge Shape
Econosnap Fascia
Drain-Thru Gravel Stop
FRAG1
Gable Edge Screen Vortex Suppressor
Gable Edge Vortex Cap Suppressor (2.375 in)
Gable Edge Vortex Cap Suppressor (.5 in)
10
5
0
-5
-10
-15
-20
1
2
3
4
5
6
7
Cp
Cpmin
Cpmean
Cprms
Edge Shapes

(h)

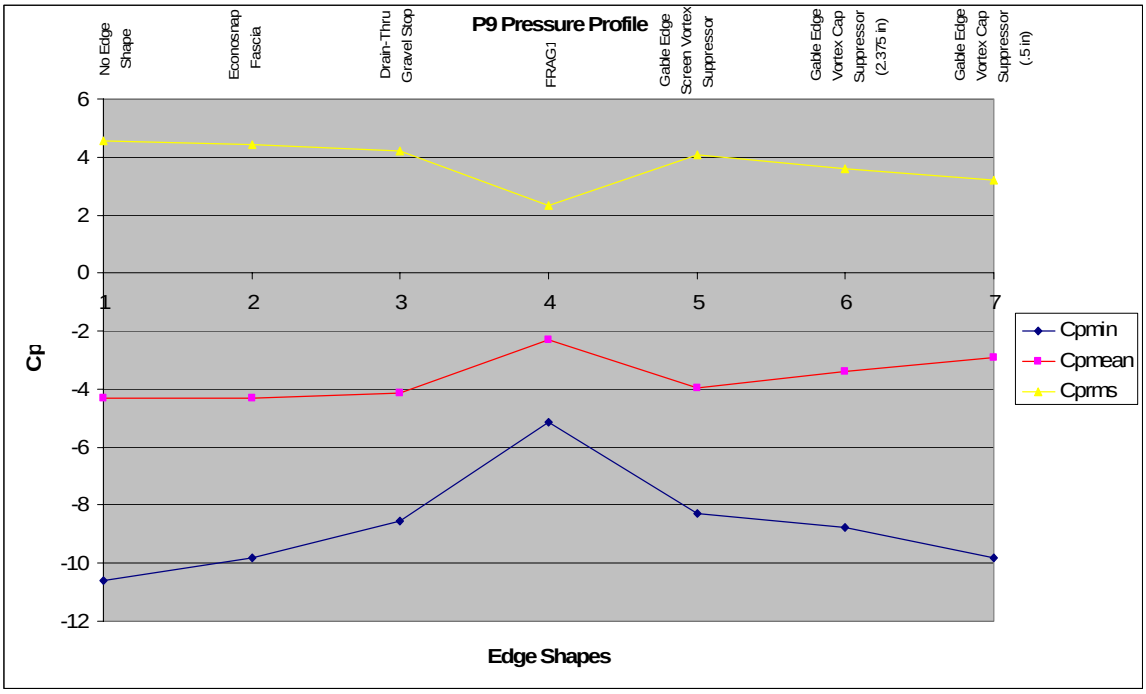
P9 Pressure Profile
No Edge Shape
Econosnap Fascia
Drain-Thru Gravel Stop
FRAG1
Gable Edge Screen Vortex Suppressor
Gable Edge Vortex Cap Suppressor (2.375 in)
Gable Edge Vortex Cap Suppressor (.5 in)
Cp
Edge Shapes
Cpmin
Cpmean
Cprms

(i)

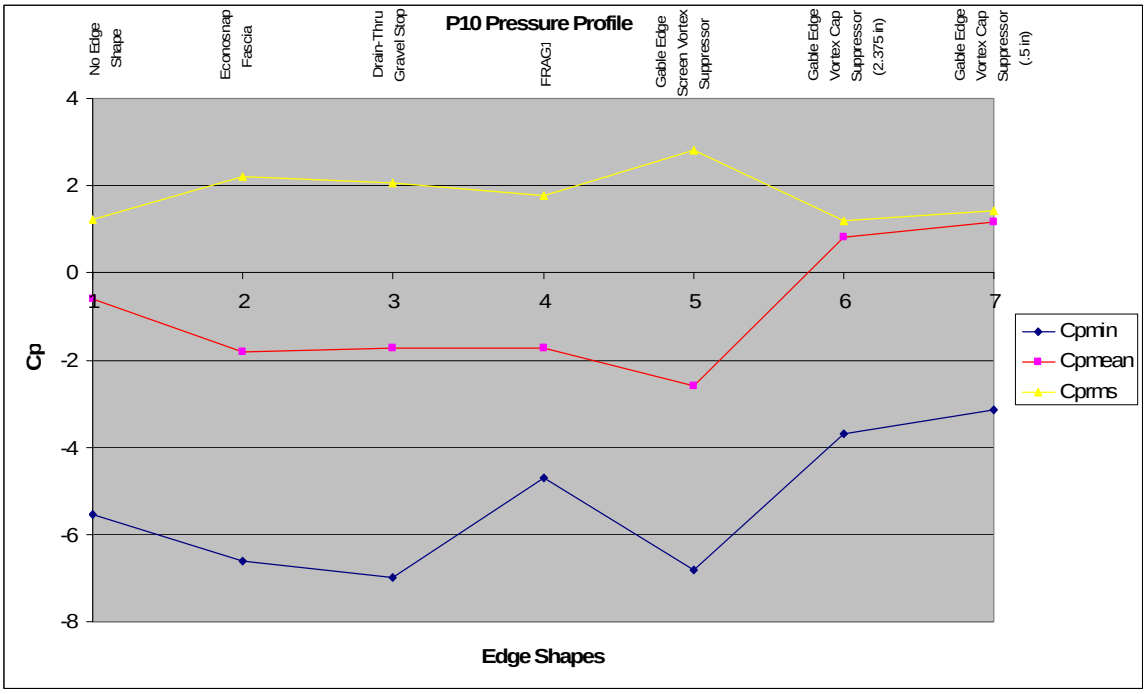
P10 Pressure Profile
No Edge Shape
Econosnap Fascia
Drain-Thru Gravel Stop
FRAG1
Gable Edge Screen Vortex Suppressor
Gable Edge Vortex Cap Suppressor (2.375 in)
Gable Edge Vortex Cap Suppressor (.5 in)
Cp
Edge Shapes
Cpmin
Cpmean
Cprms

(j)

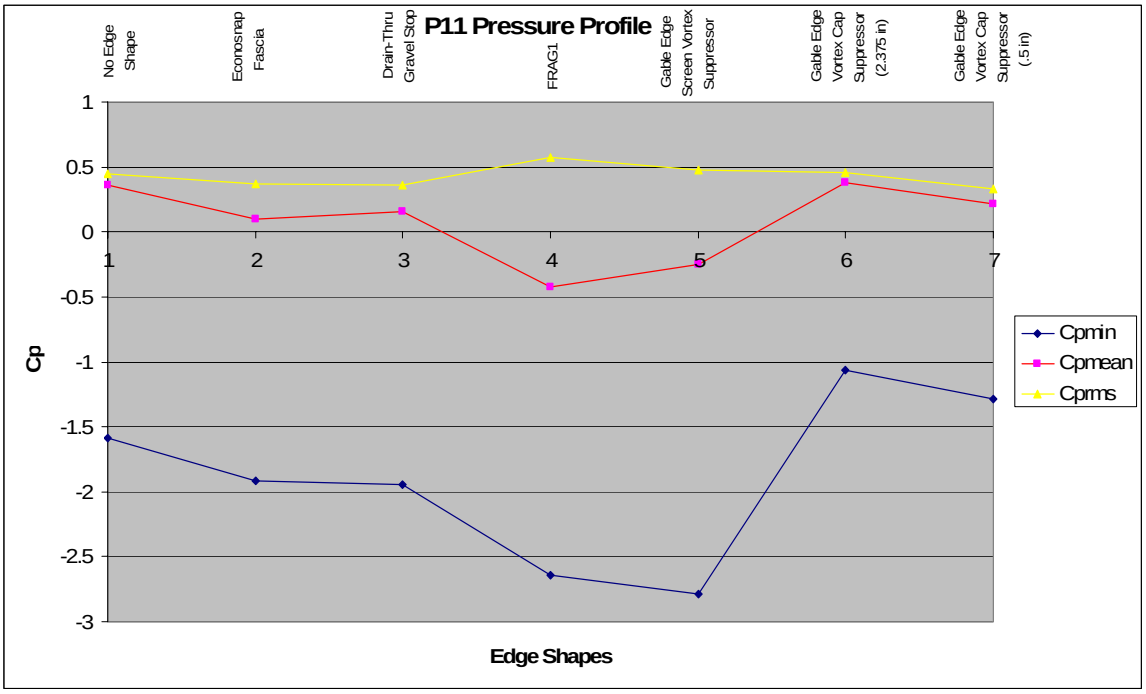
P11 Pressure Profile
No Edge Shape
Econosnap Fascia
Drain-Thru Gravel Stop
FRAG1
Gable Edge Screen Vortex Suppressor
Gable Edge Vortex Cap Suppressor (2.375 in)
Gable Edge Vortex Cap Suppressor (.5 in)
1
0.5
0
-0.5
-1
-1.5
-2
-2.5
-3
1
2
3
4
5
6
7
Cp
Edge Shapes
Cpmin
Cpmean
Cprms

(k)

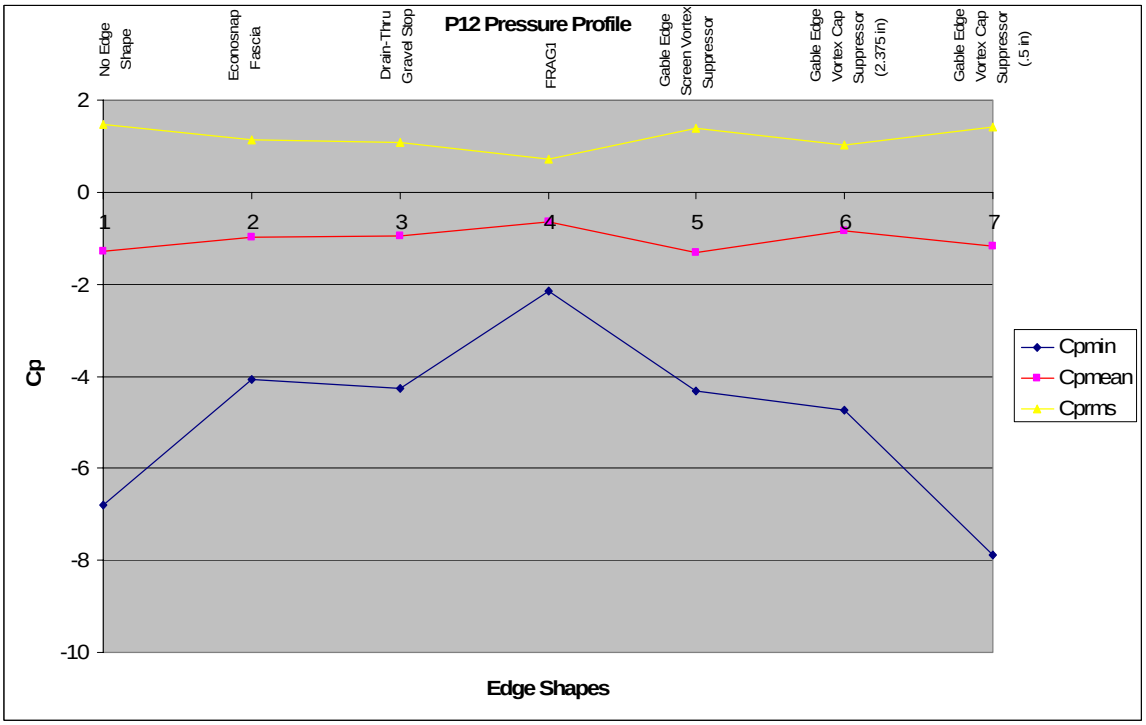
P12 Pressure Profile
No Edge Shape
Econosnap Fascia
Drain-Thru Gravel Stop
FRAG1
Gable Edge Screen Vortex Suppressor
Gable Edge Vortex Cap Suppressor (2.375 in)
Gable Edge Vortex Cap Suppressor (.5 in)
2
0
-2
-4
-6
-8
-10
1
2
3
4
5
6
7
Cp
Edge Shapes
Cpmin
Cpmean
Cprms

(l)

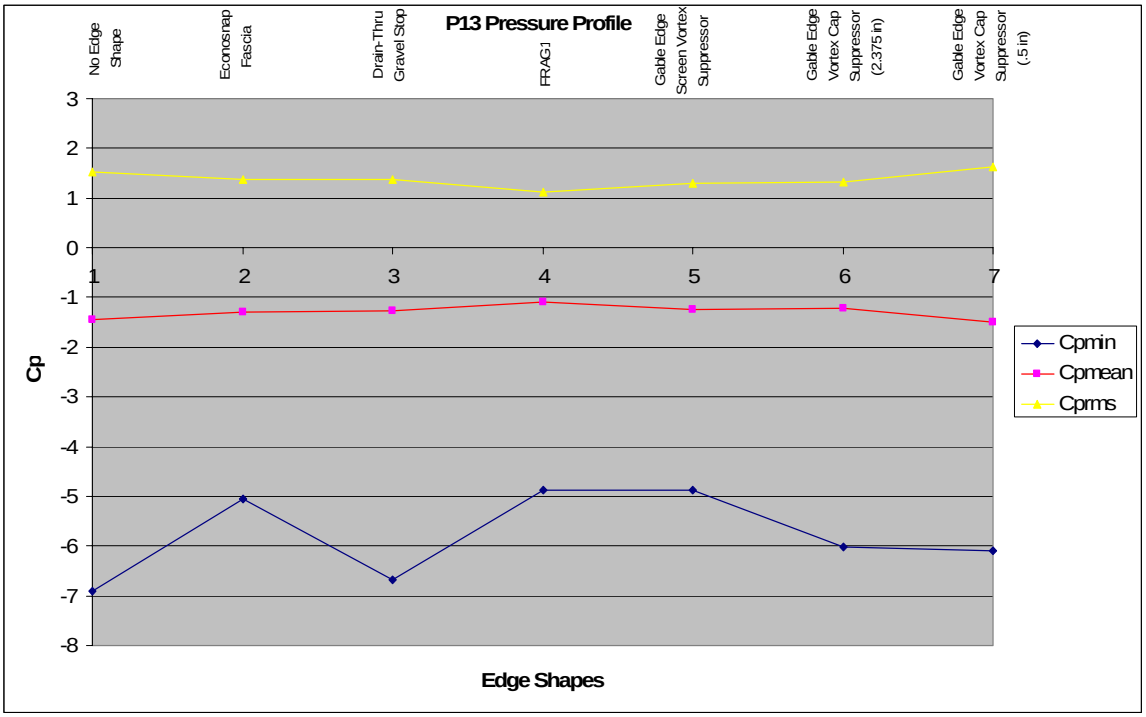
P13 Pressure Profile
No Edge Shape
Econosnap Fascia
Drain-Thru Gravel Stop
FRAG1
Gable Edge Screen Vortex Suppressor
Gable Edge Vortex Cap Suppressor (2.375 in)
Gable Edge Vortex Cap Suppressor (.5 in)
Cp
Edge Shapes
Cpmin
Cpmean
Cprms

(m)

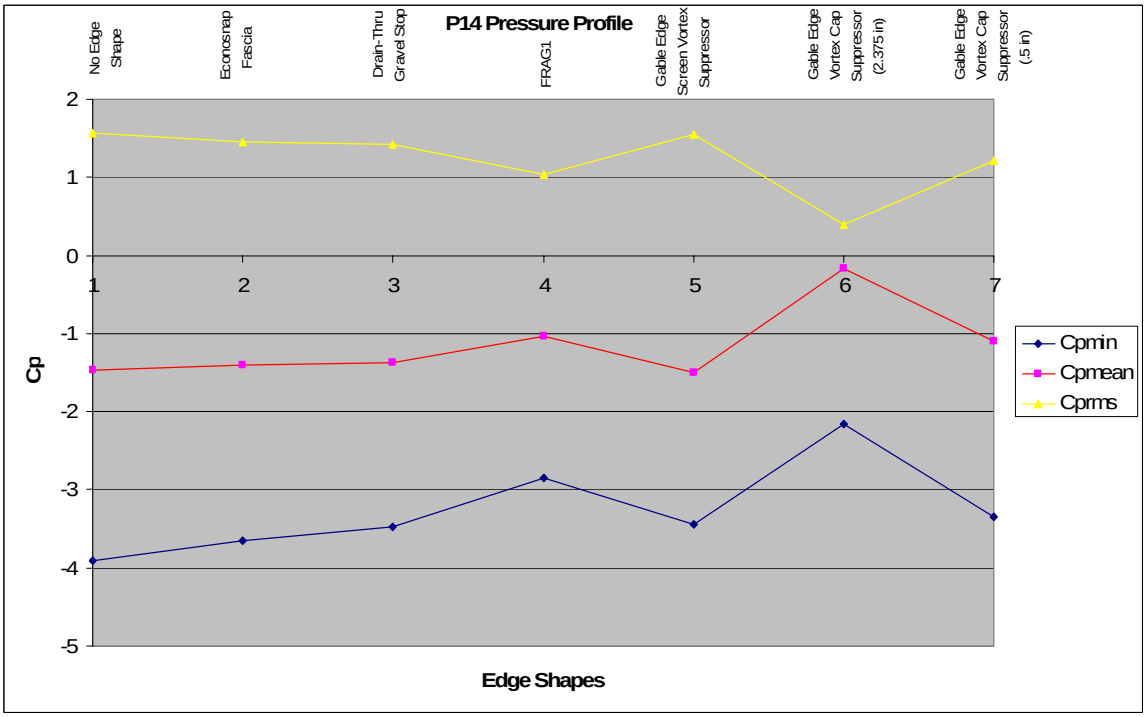
P14 Pressure Profile
No Edge Shape
Econosnap Fascia
Drain-Thru Gravel Stop
FRAG1
Gable Edge Screen Vortex Suppressor
Gable Edge Vortex Cap Suppressor (2.375 in)
Gable Edge Vortex Cap Suppressor (.5 in)
Cp
Edge Shapes
Cpmin
Cpmean
Cprms

(n)

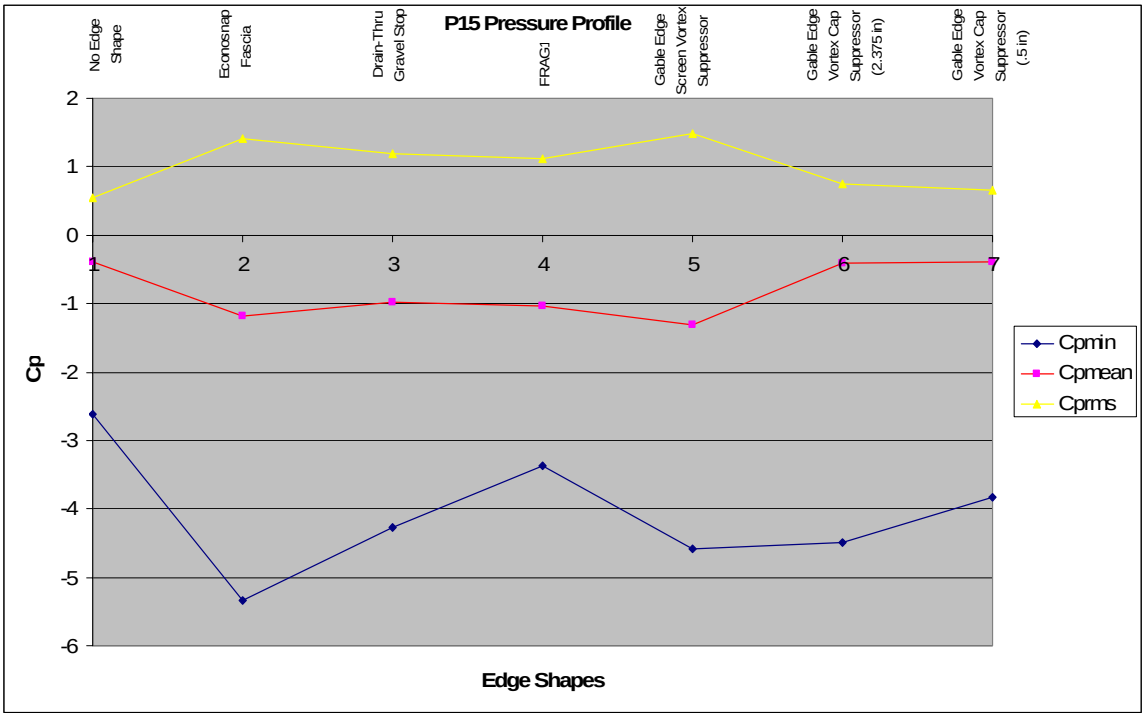

(o)

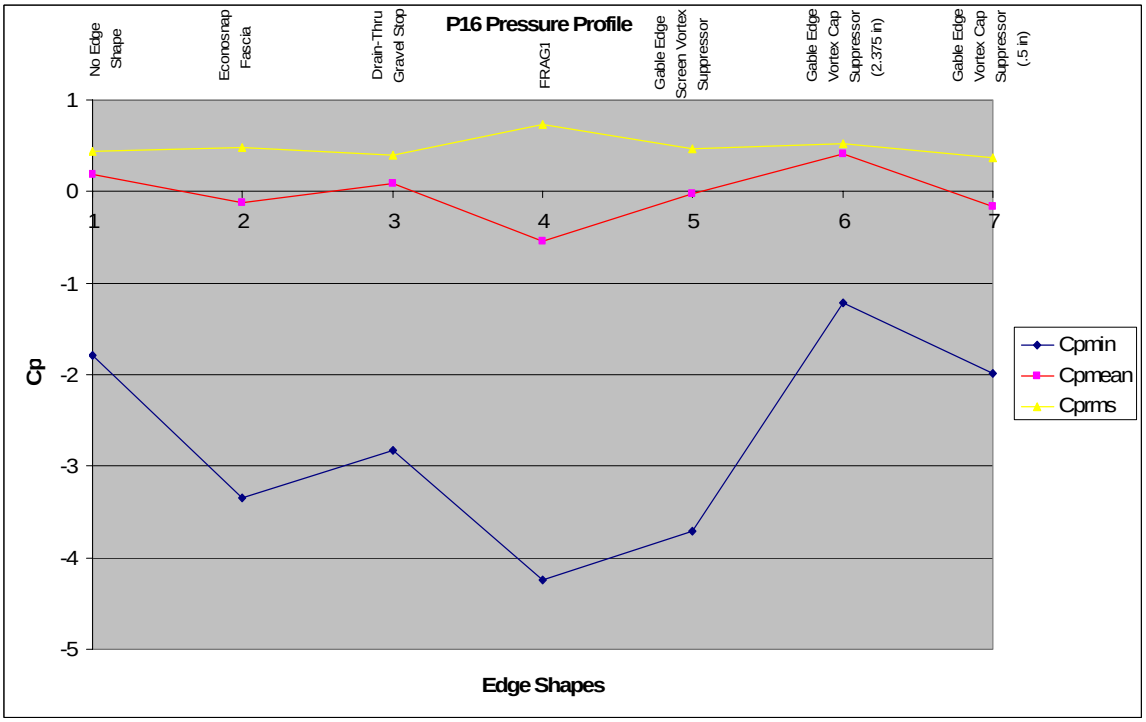

(p)

Figure 37. Response of Individual Pressure Taps to each Edge Shape Configuration

ASCE 7-05 Comparison

In order to compare WOW pressure data with ASCE 7-05 design values, design wind pressures for components and cladding (C&C) were first calculated for the test structure. Calculations are shown below.

For components and cladding:

$$q = 0.00256 * K_z * K_{zt} * K_d * I * V^2 \quad \text{(Eq. 2)}$$

Where K_z=exposure factor; K_{zt}=topographic factor; K_d=directionality factor; I=importance factor; V=basic design wind speed.

$$p_s = q[(GC_p) - (GC_{pi})] \quad \text{(Eq. 3)}$$

Where GC_p=external pressure coefficient; GC_{pi}=internal pressure coefficient.

In this case, the test structure was considered to be a partially-opened (according to ASCE 7-05 specification) residential structure in flat terrain making the importance factor, I, and the terrain factor, K_{zt}, both equal to one. The directionality factor, K_d, equals 0.85 which is the constant used with ASCE 7-05 load combinations. Finally, the basic wind speed value, V, used to calculate the design pressure is assumed to be 146 mph, the 3-sec gust design wind speed for Miami-Dade County in South Florida. Using these values, "q" is calculated and plugged into the formula to obtain P_s. For our application the internal pressure, GC_{pi} will be equal to zero for the partially enclosed case

and GC_p, the external pressure, will vary depending on the zone for which pressure is calculated. In this particular case, GC_{pi} is considered to be zero because the internal pressure of the test structure is not considered; therefore, in order for the values in the study to be comparable to ASCE 7-05 design values, this adjustment must be made. Design pressure values for the C&C can be found in Table 2.

.

Table 2. Design Pressures (psf) for the Component and Cladding

Design Zone	**Zone 1, 2 & 3**	**Interior Zone 1**	**End Zone 2**	**End Zone 3**
Pressure	11.8	-39.4	-70.9	-110.2

In order to compare these values with data measured during WOW testing, the pressure coefficients for the case with no edge shape attached had to be converted back to psf using 146 mph as the velocity value for the conversion. Because the original pressure coefficients were based on a 6-min mean wind speed, the 146 mph 3-sec gust was converted to a 6-min mean wind speed value of 107.96 mph. The minimum $C_{p\ min}$ values recorded for each tap in the no-edge-shape case were converted back to psf and the results of this conversion can be seen in Table 3.

Table 3. Equivalent pressure Values from WOW No Edge Shape Pressure Testing

Tap Number	$C_{p\ min}$	Design Pressure (psf)
P1	-7.002	-201.904
P2	-5.696	-164.249
P3	-18.231	-525.680
P4	-12.553	-361.964
P5	-8.585	-247.543
P6	-4.208	-121.340
P7	-17.985	-518.592
P8	-14.270	-411.450
P9	-10.596	-305.519
P10	-5.540	-159.749
P11	-1.584	-45.675
P12	-6.800	-196.064
P13	-6.909	-199.215
P14	-3.905	-112.590
P15	-2.617	-75.471
P16	-1.784	-51.452

For taps 1-11 located in End Zone 3, the pressures recorded during WOW testing in most cases far exceeded the design values specified by ASCE 7-05. Only 1 taps out of the 11 located in this region experienced pressures in the range of the design values. The largest difference in design values occurred at tap 3 which recorded a minimum pressure value of -525.6805 psf, almost four times the -110.2 psf value suggested in the code. Taps 12-15 also saw much lower negative pressures than the End Zone 2 design pressures suggested. Tap 16, the only tap located in interior Zone 1, recorded a minimum pressure of -51.452 psf which was still more negative than the -39.4 psf design value indicating that even regions classified as interior zones are potentially under-designed. These results are consistent with recent full-scale vs. wind tunnel studies which have suggested that pressures recorded in the full-scale are usually at least double those recorded in the wind tunnel under similar conditions. This comparison suggests that the ASCE 7-05 values should be reviewed as they may not be conservative enough, specifically in designing homes in the High-Velocity Hurricane Wind Zone. With the help of full-scale testing,

more conservative pressure design values could implemented in future versions of ASCE 7. Also, because of the success of the aerodynamic edge shapes in reducing roof suction, these retrofits could easily be considered as acceptable modifications for applying less negative design pressures for Edge Zone 3 design and construction.

6. Conclusions

Gravel scour testing and pressure testing were conducted and determined that the presence of modified edge shapes alter the physical structure of conical vortices as well as reduce the extreme suctions associated with cornering winds. The largest reduction was seen with the FRAG1 aerodynamic edge shape which resulted in a 74% reduction in peak pressures at the roof corner and a 65% reduction in mean pressure values. Because these products were so successful in testing, it is the hope of the author that they will become available for public use as a valuable and cost-effective method for reducing roof damage caused by hurricane-force winds.

References

Banks, D., Meroney, R.N., Sarkar, P.P., Zhao, Z., 2000. "Flow Visualization of Conical Vortices on Flat Roofs and Simultaneous Surface Pressure Measurement." *Journal of Wind Engineering and Industrial Aerodynamics,* Vol. 84, pp. 65-85.

Baskaran, A. & Stathopoulos, T., 1988. "Roof Corner Pressure Loads and Parapet Configurations." *Journal of Wind Engineering and Industrial Aerodynamics*, Vol. 29, pp. 79-88.

Bell, G. & Chelliah, M., 2006. "Leading Tropical Modes Associated with Interannual and Multidecadal Fluctuations in North Atlantic Hurricane Activity." *Journal of Climate*, Vol. 19 (4), pp. 590-612.

Franklin, J., Pasch, R., Avila, L., Bevin, J., Lawrence, M., Stewart, S., Blake, E., 1999. *Annual Summary: Atlantic Hurricane Season 2004.* Tropical Prediction Center, National Hurricane Center, NOAA/NWS, Miami, Fl.

Goldenburg, S.B., Landsea, C.W., Mestas-Nunez, A.M., Gray, W.M., 2001. "The Recent Increase in Atlantic Hurricane Activity: Causes and Implications." *Science*, Vol. 293, pp. 474-479.

Ho, T.C.E., Davenport, A.G., Surry, D., 1995. "Characteristic Pressure Distribution Shapes and Load Repetitions for the Wind Loading of Low Building Roof Panels." *Journal of Wind Engineering and Industrial Aerodynamics*, Vol. 57, pp. 261-279.

Irwin, H.P.A.H., Cooper, K.R., Girard, R., 1979. "Correction of Distortion Effects Caused by Tubing Systems in Measurements of Fluctuating Pressures." *Journal of Industrial Aerodynamics*, Vol. 5 (1-2), pp. 93-107.

Kawai, H. & Nishimura, G., 1996. "Characteristics of Fluctuating Suction and Conical Vortices on a Flat Roof in Oblique Flow." *Journal of Industrial Aerodynamics*, Vol. 60, pp. 211-225.

Kopp, G.A., Surry, D., Mans, C., 2005. "Wind Effects of Parapets on Low Buildings: Part 1. Basic Aerodynamics and Local Loads." *Journal of Wind Engineering and Industrial Aerodynamics*, Vol. 93, pp. 817-841.

Kopp, G.A., Mans, C., Surry, D., 2005. "Wind Effects of Parapets on Low Buildings: Part 2. Structural Loads." *Journal of Wind Engineering and Industrial Aerodynamics*, Vol. 93, pp. 843-855.

Kopp, G.A., Mans, C., Surry, D., 2005. "Wind Effects of Parapets on Low Buildings: Part 4. Mitigation of Corner Loads with Alternative Geometry." *Journal of Wind Engineering and Industrial Aerodynamics*, Vol. 93, pp. 843-855.

Landsea, W., Pielke, R., Mestas-Nunez, A., Knaff, J., 1999. "Atlantic Basin Hurricanes: Indices of Climatic Change." *Climatic Change*, Vol. 42, pp 89-129.

Levitan, M.L. & Mehta, K.C., 1992. "Texas Tech Field Experiments for Wind Loads Part 1: Building and Pressure Measuring System." *Journal of Wind Engineering and Industrial Aerodynamics*, Vol. 43, pp. 1565-1576.

Levitan, M.L. & Mehta, K.C., 1992. "Texas Tech Field Experiments for Wind Loads Part II: Meteorological Instrumentation and Terrain Parameters." *Journal of Wind Engineering and Industrial Aerodynamics*, Vol. 43, pp. 1577-1588.

Levitan, M.L., Mehta, K.C., Vann, W.P., 1991. "Field Measurements of Pressures on the Texas Tech Building." *Journal of Wind Engineering and Industrial Aerodynamics*, Vol. 38, pp. 227-234.

Lin, J.X., Surry, D., Tieleman, H.W., 1995. "The Distribution of Pressure Near Roof Corners of Flat Roof Low Buildings." *Journal of Wind Engineering and Industrial Aerodynamics*, Vol. 56, pp. 235-265.

Lin, J.X. & Surry, D., 1998. "The Variation of Peak Loads with Tributary Area Near Corners on Flat Low Building Roofs." *Journal of Wind Engineering and Industrial Aerodynamics*, Vol. 77-78, pp. 185-196.

Lott, N., & Ross, T., 2006. "Tracking and Evaluating U.S. Billion Dollar Weather Disasters. 1980-2005." NOAA National Climatic Data Center, Asheville, N.C.

Mans, C., Kopp, G., Surry, D., 2005. "Wind Effects of Parapets on Low Buildings: Part 3. Parapet Loads." *Journal of Wind Engineering and Industrial Aerodynamics*, Vol. 93, pp. 857-872.

Melbourne, W.H. & Cheung, J.C.K., 1988. "Reducing Wind Loading on Large Cantilevered Roofs." *Journal of Wind Engineering and Industrial Aerodynamics*, Vol. 28, pp. 401-410.

Mehta, K.C., Levitan, M.L., Iverson, R.E., McDonald, J.R., 1992. "Roof Corner Pressures Measured in a Field on a Low Building." *Journal of Wind Engineering and Industrial Aerodynamics*, Vol. 41-44, pp. 181-192.

Sarkar, P., Zhao, Z., Mehta, K.C., 1997. "Flow Visualization and Measurement on the Roof of the Texas Tech Building." *Journal of Wind Engineering and Industrial Aerodynamics*, Vol. 69-71, pp. 597-606.

Stathopoulos, T., Baskaran, A., Goh, P.A., 1990. "Full-Scale Measurements of Wind Pressures on Flat Corner Roofs." *Journal of Wind Engineering and Industrial Aerodynamics*, Vol. 36, pp. 1063-1072.

Stathopoulos, T., Marathe, R., Wu, H., 1999. "Mean Wind Pressures on Flat Roof Corners Affected by Parapets: Field and Wind Tunnel Studies." *Engineering Structures*, Vol. 21, pp. 629-638.

Surry, D. & Lin, J.X., 1995. "The Effect of Surroundings and Roof Corner Geometris Modifications on Roof Pressures on Low-Rise Buildings." *Journal of Wind Engineering and Industrial Aerodynamics*, Vol. 58, pp. 113-138.

Tieleman, H.W., Surry, D., Lin, J.X., 1994. "Characteristics of Mean and Fluctuating Pressure Coefficients Under Corner (Delta-Wing) Vortices." *Journal of Wind Engineering and Industrial Aerodynamics*, Vol. 52, pp. 263-275.

Wu, F., Sarkar, P., Mehta, K.C., Zhao, Z., 2001. "Influence of Incident Wind Turbulence on Pressure Fluctuations Near Flat-Roof Corners." *Journal of Wind Engineering and Industrial Aerodynamics*, Vol. 89, pp. 403-420.

Wu, F., 2000. *Full-Scale Study of Conical Vortices and Their Effects Near Roof Corners.* Doctoral Dissertation, Department of Civil Engineering, Texas Tech University.

Yang, H., Sims-Williams, D.B., He, L., 2006. "Unsteady Pressure Measurement with Correction on Tubing Distortion." Unsteady Aerodynamics, Aeroacoustics and Aeroelasticity of Turbomachines, Netherlands, pp 521-529.

Zhao, Z., 1997. *Wind Flow Characteristics and Their Effects on Low-Rise Buildings.* Doctoral Dissertation, Department of Civil Engineering, Texas Tech University.

Zhu, H., 2006. *C-130 Testings on Low-Rise Buildings.* Doctoral Dissertation, Department of Civil Engineering, Texas Tech University.

Appendices

Appendix A. Three-Dimensional Plots of Pressure Coefficients for Each Edge Shape

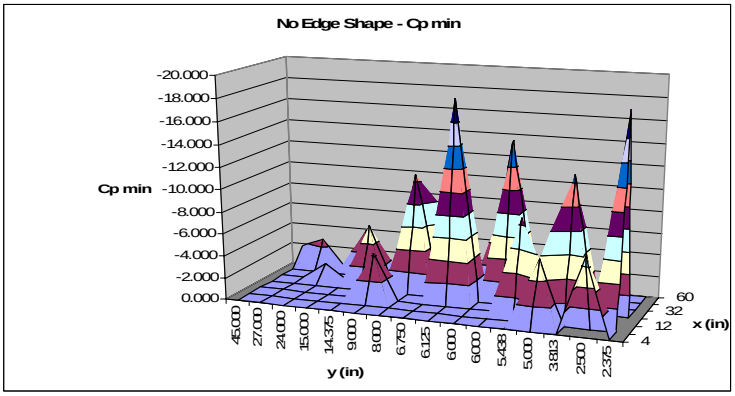

(a)

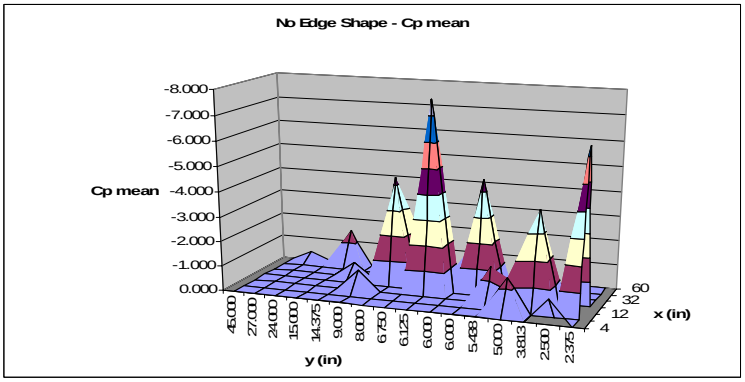

(b)

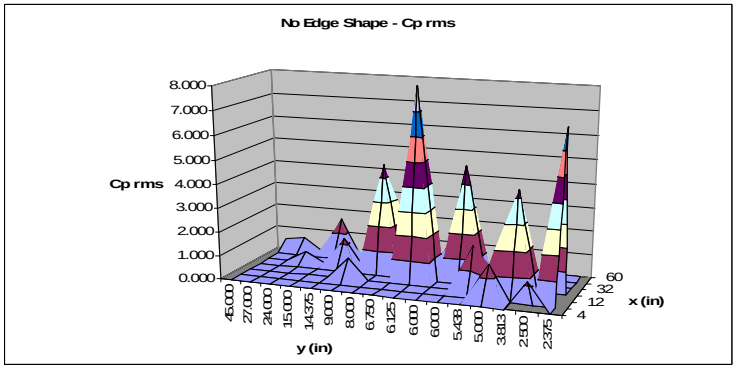

(c)

Figure 38. Cp Distribution for No Edge Shape Case

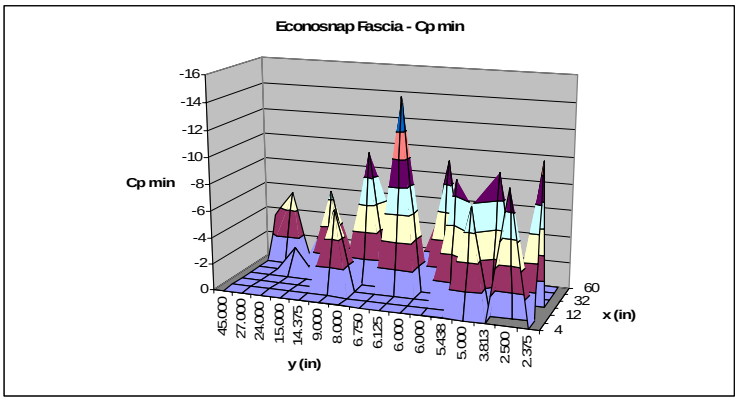

(a)

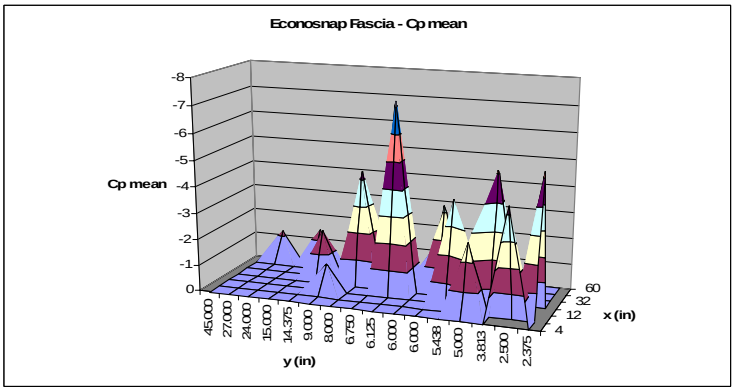

(b)

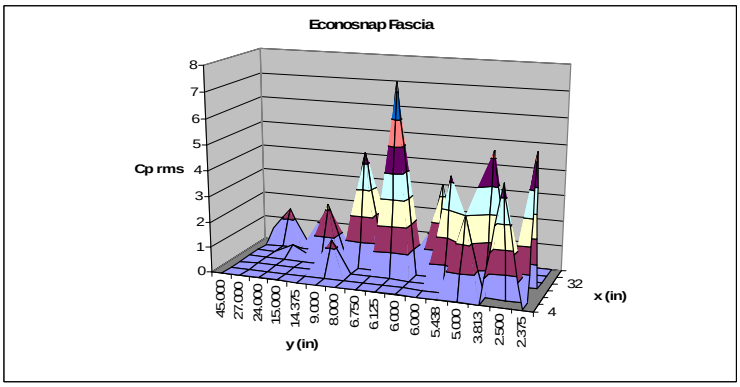

(c)

Figure 39. Cp Distribution for Econosnap Fascia Case

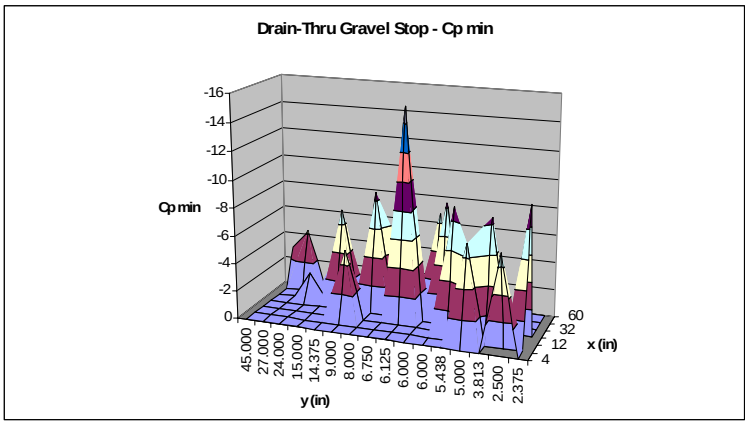

(a)

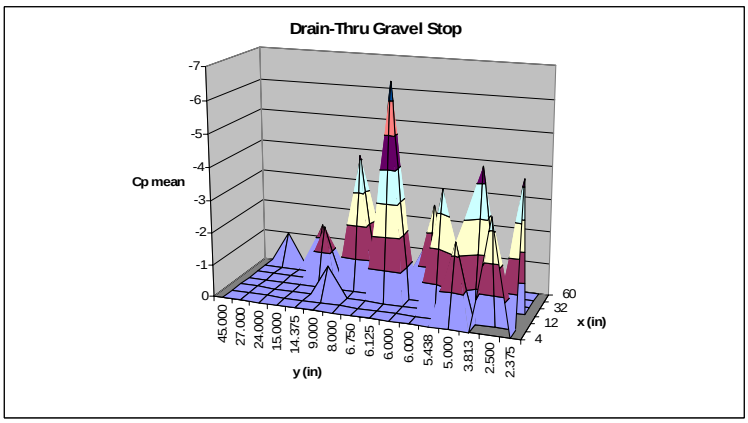

(b)

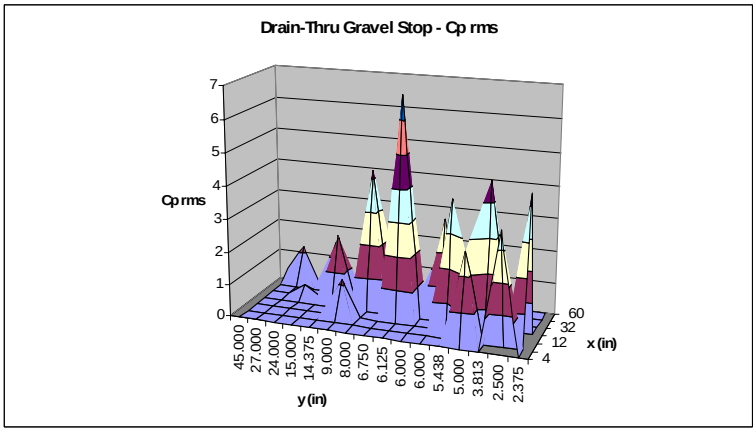

(c)

Figure 40. Cp Distribution for Drain-Thru Gravel Stop Case

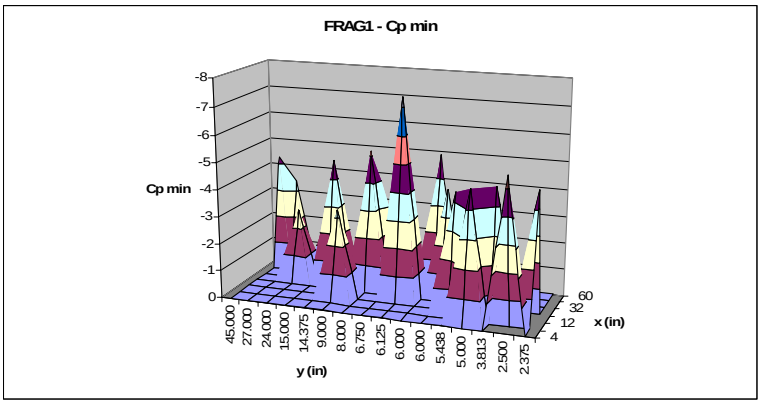

(a)

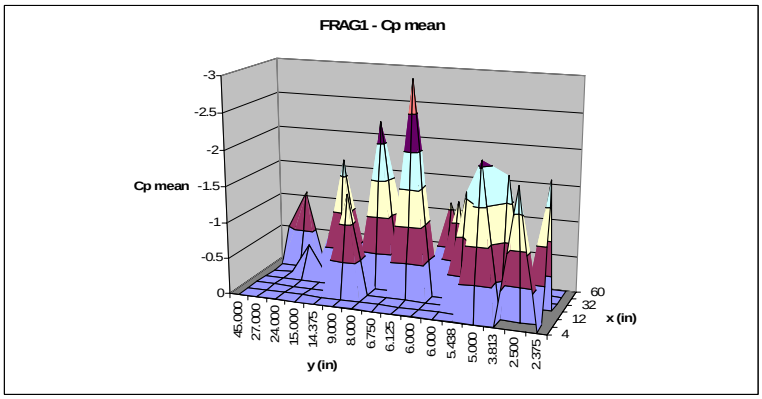

(b)

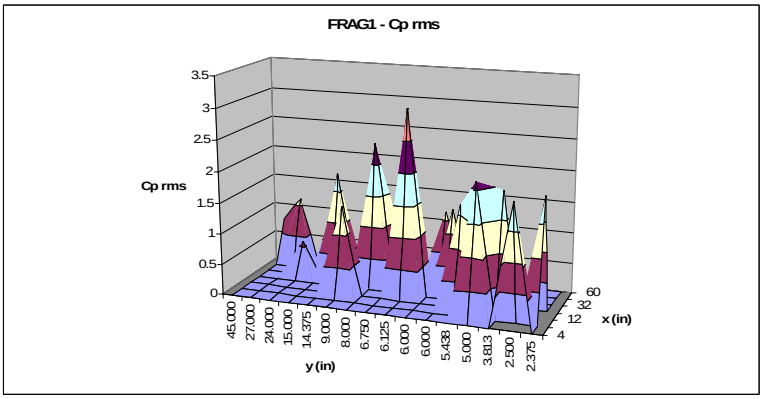

(c)

Figure 41. Cp Distribution for FRAG1 Edge Shape Case

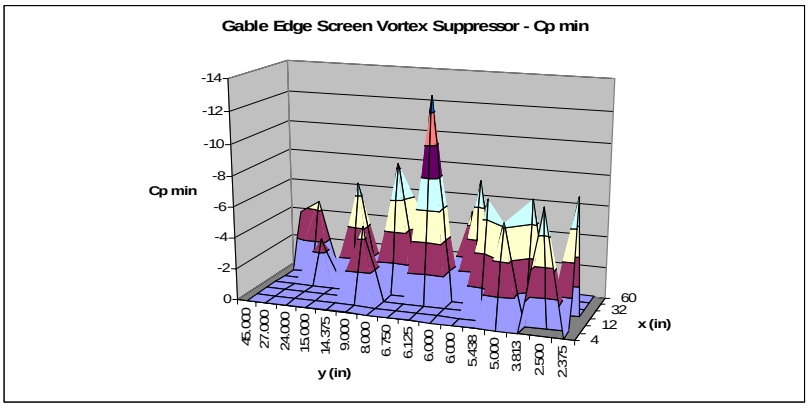

(a)

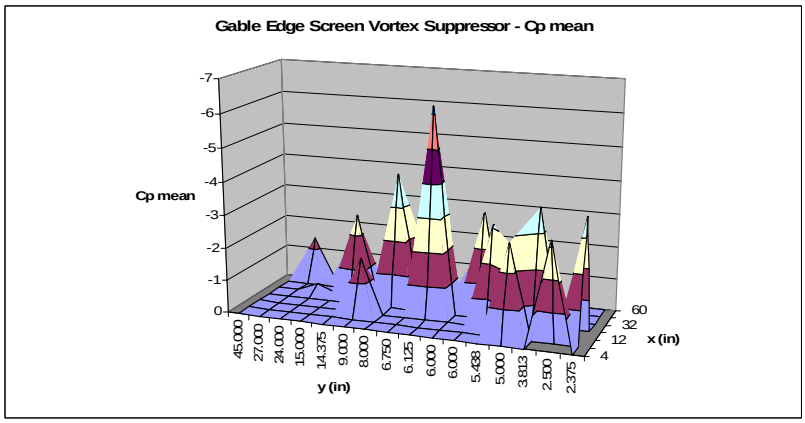

(b)

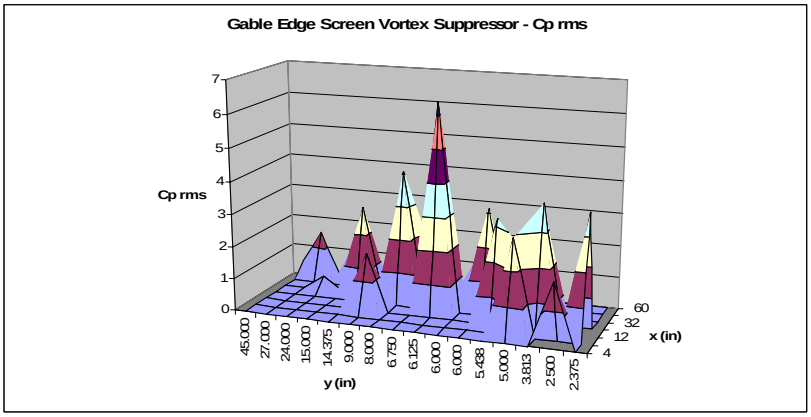

(c)

Figure 42. Cp Distribution for Gable Edge Screen Vortex Suppressor Case

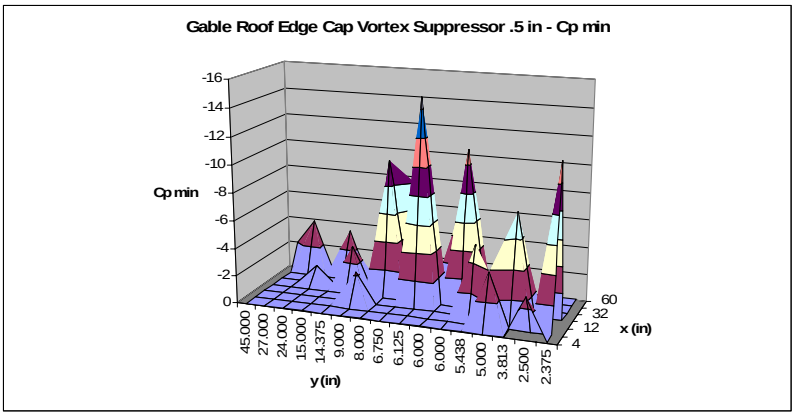

(a)

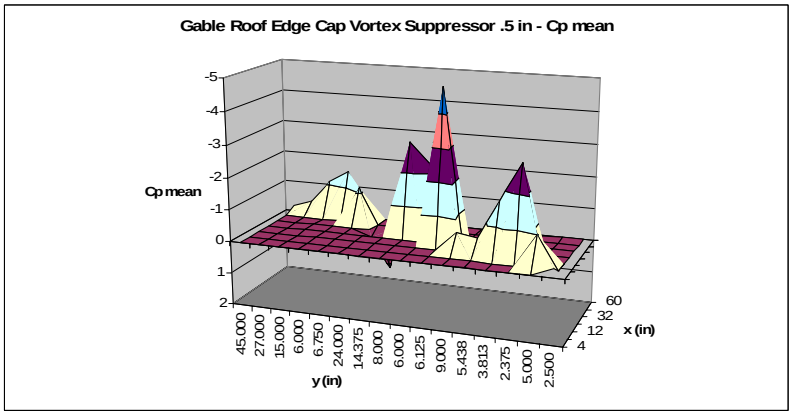

(b)

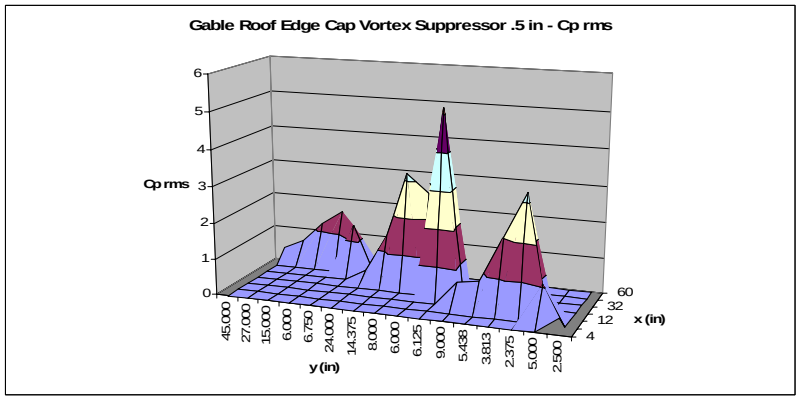

(c)

Figure 43. Cp Distribution for Gable Roof Edge Cap Vortex Suppressor 0.5 in Case

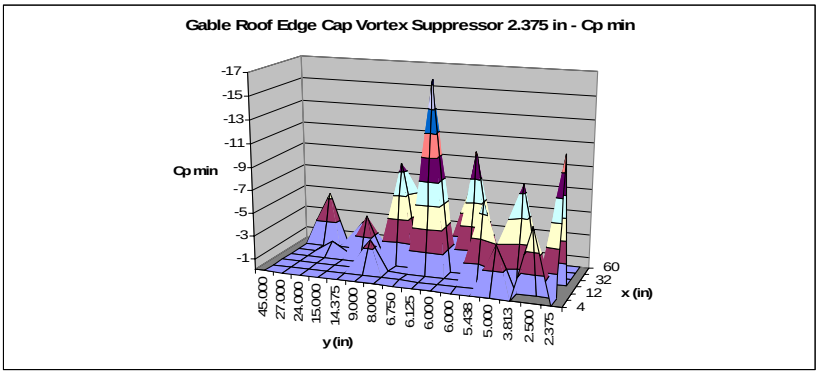

(a)

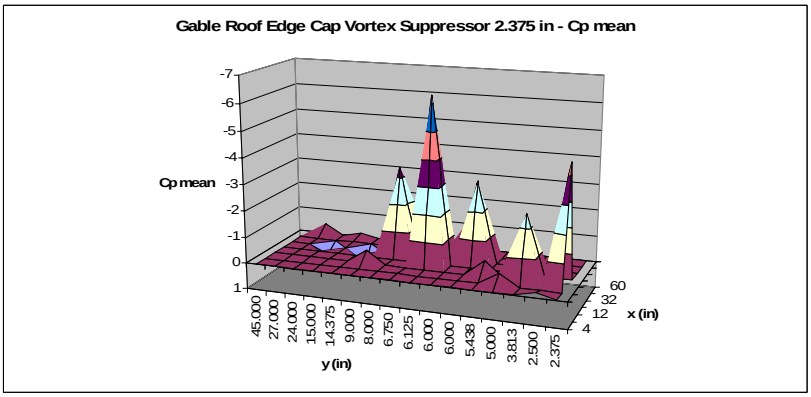

(b)

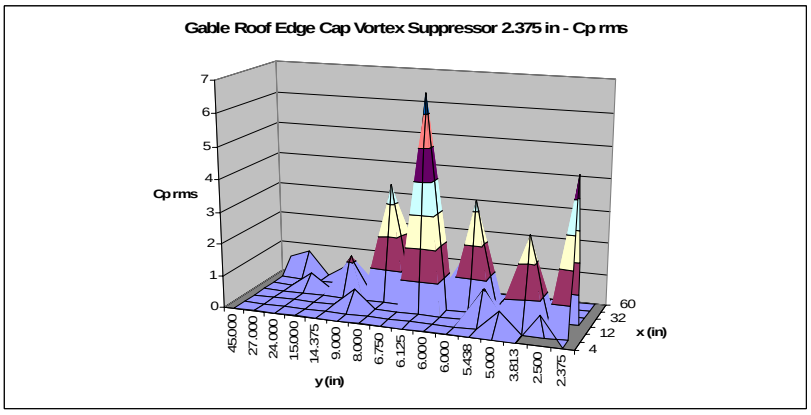

(c)

Figure 44. Cp Distribution for Gable Roof Cap Vortex Suppressor 2.375 in Case

Appendix B. Comparison of Edge Shape Results

Table 2. (a) Comparison of Edge Shape Results

	No Edge Shape			Econosnap Fascia			Drain-Thru Gravel Stop			FRAG1		
Pressure Taps	C_{pmin}	C_{pmean}	C_{prms}	C_{pmin}	C_{pmean}	C_{prms}	C_{pmin}	C_{pmean}	C_{prms}	C_{pmin}	C_{pmean}	C_{prms}
P1	-7.002257	-0.987882	1.189699	-9.762437	-4.297326	4.534117	-7.048982	-3.438283	3.591512	-5.47226	-1.87879	1.971288
P2	-5.696362	-1.382497	1.483507	-7.767984	-2.669616	3.008443	-6.936135	-2.391402	2.679832	-4.724319	-2.092175	2.129993
P3	-18.23122	-6.406206	6.89124	-11.02373	-5.214343	5.36728	-9.623359	-4.220891	4.356821	-4.7006	-1.834638	1.921616
P4	-12.55335	-3.859905	4.322562	-9.894352	-5.143631	5.279021	-8.484963	-4.494426	4.614985	-4.663692	-1.852215	1.939426
P5	-8.585067	-1.491522	1.907509	-9.150992	-3.93981	4.218787	-8.901868	-3.700069	3.951482	-4.317446	-1.577574	1.663787
P6	-4.208205	-0.822062	0.905567	-6.129841	-1.049333	1.27142	-4.959807	-0.947704	1.13505	-3.286078	-1.402934	1.441747
P7	-17.98538	-7.620039	7.995003	-14.42355	-7.186515	7.377705	-15.17883	-6.557022	6.738208	-7.358909	-2.954763	3.008345
P8	-14.26957	-4.47256	4.756865	-9.702084	-3.236601	3.426891	-8.31299	-2.82138	2.995233	-3.965759	-1.284586	1.374365
P9	-10.59575	-4.322913	4.558504	-9.829516	-4.30921	4.438899	-8.559594	-4.118536	4.225662	-5.138687	-2.300456	2.335634
P10	-5.540294	-0.591554	1.217096	-6.614832	-1.825691	2.196048	-6.980623	-1.737279	2.076405	-4.7066	-1.719888	1.785105
P11	-1.584066	0.356899	0.451382	-1.919106	0.103908	0.369	-1.948024	0.158277	0.356708	-2.64235	-0.428258	0.570253
P12	-6.799717	-1.277438	1.463792	-4.078413	-0.985344	1.138479	-4.260488	-0.956802	1.079304	-2.158182	-0.653374	0.706648
P13	-6.90901	-1.445012	1.522938	-5.061063	-1.283291	1.362992	-6.674315	-1.265973	1.385499	-4.86714	-1.093973	1.122835
P14	-3.904749	-1.474583	1.569026	-3.646864	-1.395982	1.458471	-3.474784	-1.366546	1.424262	-2.853335	-1.033359	1.043948
P15	-2.617428	-0.387114	0.555126	-5.336679	-1.189723	1.408175	-4.267126	-0.977105	1.191845	-3.36349	-1.042191	1.111432
P16	-1.784404	0.182699	0.441325	-3.349577	-0.126671	0.475071	-2.825651	0.094426	0.391928	-4.244256	-0.540177	0.729403

Table 2. (b) Comparison of Edge Shape Results (continued)

	Gable Edge Vortex Screen			Gable Edge Vortex Cap (.5")			Gable Edge Vortex Cap (2.375")		
Pressure Taps	C_{pmin}	C_{pmean}	C_{prms}	C_{pmin}	C_{pmean}	C_{prms}	C_{pmin}	C_{pmean}	C_{prms}
P1	-7.808025	-3.210488	3.314741	-3.019683	-0.269744	0.441077	-6.335841	-0.204942	0.903745
P2	-6.244241	-2.824306	2.906344	-3.888649	-1.004812	1.068265	-3.980599	-0.444405	0.632722
P3	-7.839338	-3.594034	3.69466	-11.57071	-2.867889	3.268638	-11.47357	-4.449758	4.695235
P4	-7.48247	-3.712056	3.815582	-7.816634	-1.688476	2.013828	-8.746685	-2.470096	2.835739
P5	-7.268304	-3.102928	3.221118	-5.199906	-0.501249	0.773624	-6.974151	-0.591644	1.046616
P6	-4.736261	-1.673175	1.786828	-2.189126	-0.625758	0.686197	-2.680641	-0.488818	0.586364
P7	-12.99442	-6.235862	6.382626	-14.78632	-4.806131	5.162166	-16.43777	-6.294026	6.6016
P8	-7.611114	-3.022438	3.149817	-11.04355	-2.287691	2.683693	-10.24559	-3.090001	3.329185
P9	-3.705879	-0.018164	0.467492	-1.987121	-0.162901	0.364598	-1.211347	0.410044	0.518504
P10	-6.819917	-2.585959	2.810118	-3.149079	1.153209	1.416335	-3.682901	0.814532	1.181938
P11	-2.788108	-0.254237	0.475355	-1.28291	0.219379	0.333775	-1.059452	0.377363	0.461922
P12	-4.333263	-1.303951	1.382572	-7.891892	-1.166527	1.42491	-4.724668	-0.826115	1.036964
P13	-4.870589	-1.230331	1.300348	-6.085447	-1.501339	1.617665	-6.031083	-1.217926	1.320368
P14	-3.435739	-1.492764	1.544043	-3.345725	-1.104656	1.206828	-2.154497	-0.170466	0.401159
P15	-4.579161	-1.317139	1.48167	-3.837979	-0.384749	0.649025	-4.499568	-0.402535	0.747957
P16	-8.297453	-3.973233	4.072544	-9.80932	-2.916469	3.189174	-8.76115	-3.374648	3.59506

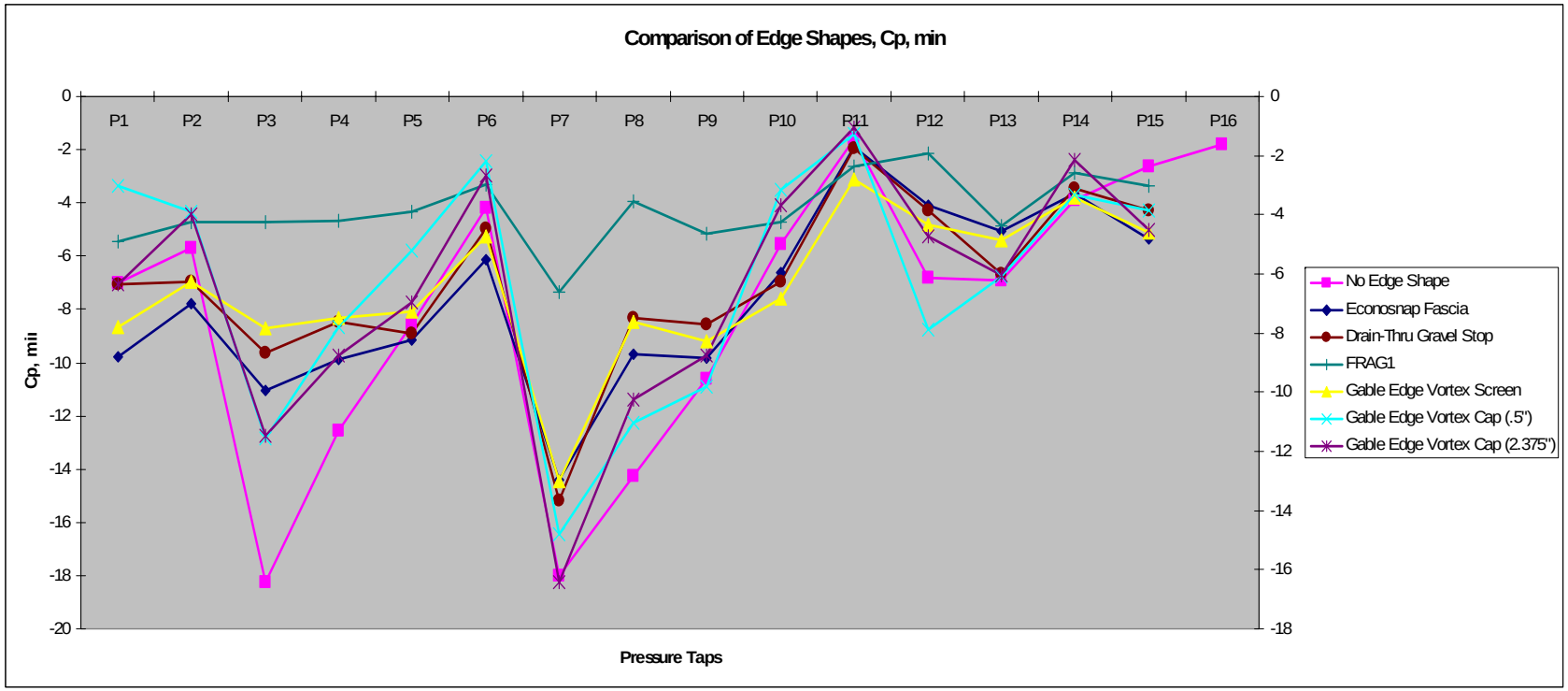

Figure 45. Comparison of $C_{p\ min}$ for all Edge Shapes

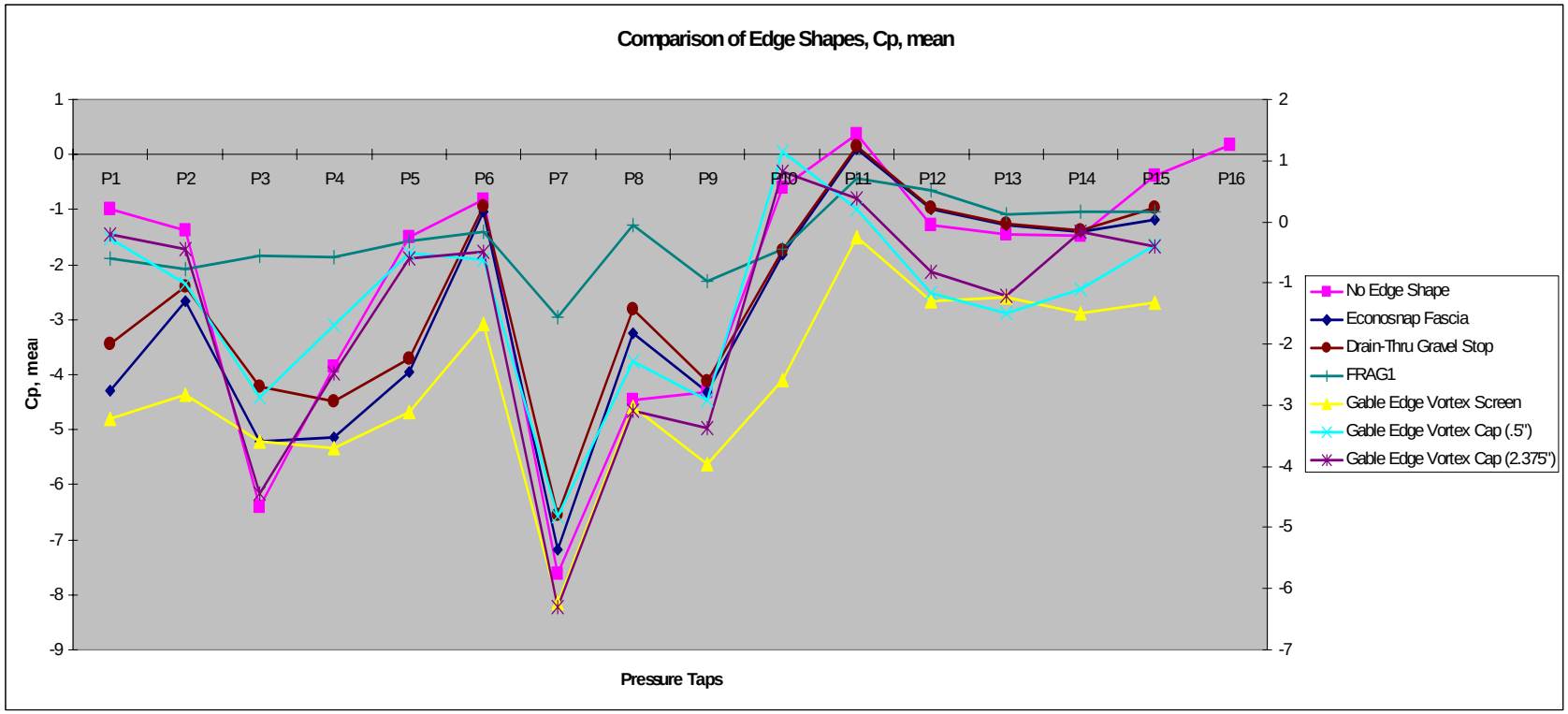

Figure 46. Comparison of $C_{p\ mean}$ for all Edge Shapes

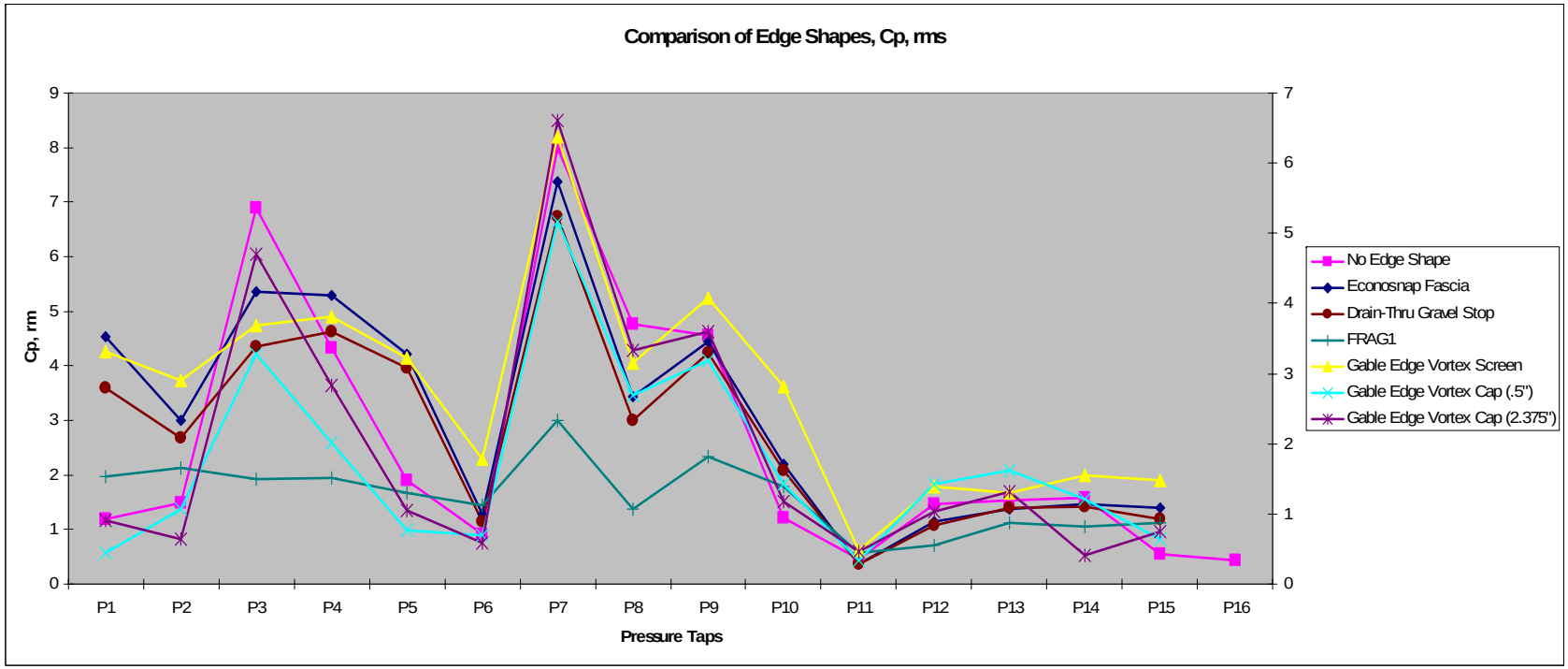

Figure 47. Comparison of $C_{p\ rms}$ for all Edge Shapes